



Original Paper

A Novel Approach to Self-potential Data Interpretation in Support of Mineral Resource Development

Mahmoud Elhussein ^{1,2}

Received 21 March 2020; accepted 29 May 2020

Published online: 16 June 2020

A new efficient technique has been developed to interpret self-potential data from different mineralized sources (horizontal cylinder, vertical cylinder, sphere, and 2-D inclined sheet). This technique is based on the first horizontal gradient filter and particle swarm optimization algorithm. This suggested method can be used for single-source and multiple-source interpretation. In this study, the developed technique was applied to five different synthetic examples (vertical cylinder model, horizontal cylinder model, sphere model, 2-D inclined sheet model, and multi-source model), using a real case from Canada—the multi-source field example—and two real cases from India. The results obtained from the synthetic and real data show that the method is fast, accurate, and effective in removing the regional background and does not require information regarding body shape. The results of the real data cases match well with the results obtained from other published methods.

KEY WORDS: Mining, Self-potential, Gradient, Particle swarm optimization, Sheet, Depth.

INTRODUCTION

The self-potential or spontaneous polarization technique is one of the most passive geophysical methods, measuring the natural potential difference (ΔV) in the subsurface that results from electrochemical, thermoelectric, and electrokinetic fields within the earth's interior (Biswas 2017; Essa 2020). There are many geophysical problems that can be solved by using the self-potential method, such as groundwater exploration, mining, geothermal investigation, archeology, paleo-shear zone detection, and cavity detection (Corwin and Hoover 1979; Wynn and Sherwood 1984; Sundararajan et al. 1998; Vichabian and Morgan 2002; Drahor 2004; Minsley et al. 2008; Fernandez-Martinez et al. 2010; Meha-

nee 2014, 2015; Essa and Elhussein 2017; Essa 2019, 2020). Since non-unique and ill-posed problems are encountered in the interpretation of self-potential anomalies caused by different mineralized sources, different inversion modeling techniques have been developed to handle these problems (Zhdanov 2002; Tarantola 2005; Biswas 2013; Biswas and Sharma 2014b; Mehane and Essa 2015; Wang 2016; Essa 2020). Inversion modeling techniques have been based upon the approximation of the different geoelectric sources with simple geometric structures (horizontal cylinder, vertical cylinder, sphere, and 2-D inclined sheet) to determine the structure parameters (Stoll et al. 1995; El-Kaliouby and Al-Garni 2009; Essa 2011, 2019; Dmitriev 2012; Sharma and Biswas 2013; Roudsari and Beitollahi 2013; Mehane 2014; Essa and Elhussein 2017; Kawada and Kasaya 2018). These techniques include the use of nomograms and the characteristic point method (Paul 1965; Bhattacharya and Roy 1981; Murthy and Haricharan 1985; Sundararajan et al. 1990; Fedi and

¹Department of Geophysics, Faculty of Science, Cairo University, P.O. 12613 Giza, Egypt.

²To whom correspondence should be addressed; e-mail: mahmoudelnouishy@yahoo.com

Abbas 2013), window curves method (Abdelrahman et al. 2006b, 2009a; Essa 2007), linear inversion modeling (Asfahani and Tlas 2016), non-linear inversion modeling (Asfahani and Tlas 2005; Abdelrahman et al. 2006a; Essa et al. 2008), horizontal gradient method (Abdelrahman et al. 2009b; Essa and Elhussein 2017), and neural networks (El-Kaliouby and Al-Garni 2009). Many of the previous methods require a priori information about the model's parameters and a suitable range for searching for the best solution for each parameter. The most recent techniques include simulated annealing (Göktürkler and Balkaya 2012), very fast simulated annealing (Sharma and Biswas 2013; Biswas and Sharma 2015; Biswas 2016), genetic algorithm (Göktürkler and Balkaya 2012), and particle swarm optimization (PSO) (Santos 2010; Göktürkler and Balkaya 2012; Essa 2019, 2020; Essa and Elhussein 2020).

In this study, a new technique based upon global PSO was developed to invert self-potential datasets for different mineralized sources (horizontal cylinder, vertical cylinder, sphere, and 2-D inclined sheet) to calculate the different models parameters, namely, amplitude coefficient (A_c), depth (h), polarization angle (α), inclination angle (β), half-width (d), shape factor (S_f), and source origin (w). The technique used here applies PSO to the first horizontal gradient anomalies of the self-potential data to remove the effect of the regional background. The proposed method was applied to five different synthetic models with and without 15% random noise and to three real cases from Canada and India.

METHODOLOGY

The measured self-potential anomaly is composed of the residual anomaly due to different mineralized sources (horizontal cylinder, vertical cylinder, sphere, and 2-D inclined sheet) and the unwanted regional anomaly, which is the measured anomaly (Essa 2020), thus:

$$\Delta V(x_i) = V_{\text{res}}(x_i, h, \alpha) + Z(x_i), \quad (1)$$

where $\Delta V(x_i)$ is the total measured self-potential anomaly, $V_{\text{res}}(x_i, h, \alpha)$ is the residual anomaly caused by different sources, and $Z(x_i)$ is the regional anomaly. In this study, the PSO algorithm was applied to invert the residual anomalies, which were

separated from the total anomalies using the first horizontal gradient.

Forward Modeling of Different Structures and the First Horizontal Gradient

The self-potential anomaly (V_{res}) for different simple geometric structures (Figs. 1a, b, c) at any point (x_i) is given by (Bhattacharya and Roy 1981; Essa 2019):

$$\begin{aligned} V_{\text{res}}(x_i, h, \alpha) &= A_c \frac{(x_i - w) \cos \alpha - h \sin \alpha}{\left((x_i - w)^2 + h^2 \right)^{S_f}}, i \\ &= 0, 1, 2, 3, \dots, M \end{aligned} \quad (2)$$

where M is number of data points, S_f is shape factor (dimensionless), h is depth of structure (m), A_c is the amplitude coefficient, (mV m^{2S_f-1}), w is position of source body (m), and α is polarization angle (degree). The S_f is dependent on the shape of the structure and is equal to 1.5 for a sphere-like structure, 1 for a horizontal cylinder-like structure, and 0.5 for a semi-infinite vertical cylinder.

The self-potential anomaly (V_{res}) caused by a 2-D inclined sheet (Fig. 1d) at any location (x_i) on a profile perpendicular to the strike of this sheet is defined as (Murthy and Haricharan 1985; Sundararajan et al. 1998; Sharma and Biswas 2013; Essa 2020):

$$\begin{aligned} V_{\text{res}}(x_i, h, \beta, d) &= A_c \ln \left[\frac{\left((x_i - w) - d \cos \beta \right)^2 + (h - d \sin \beta)^2}{\left((x_i - w) + d \cos \beta \right)^2 + (h + d \sin \beta)^2} \right], \\ &i = 0, 1, 2, 3, \dots, M \end{aligned} \quad (3)$$

where A_c is the amplitude coefficient, (mV), d is half-width, and β is sheet inclination angle.

To remove regional background, the first horizontal gradient was applied to Eq. (1) by using two different observation locations ($x_i + s$ and $x_i - s$) along the anomaly profile. The first horizontal gradient anomaly can be defined as follows:

$$\Delta V_x(x_i, s) = \frac{\Delta V(x_i + s) - \Delta V(x_i - s)}{2s}, \quad (4)$$

where $s = 1, 2, 3, \dots, N$ spacing units and is called window length or graticule spacing. The inversion algorithm was then applied to Eq. (4) to estimate the different source parameters.

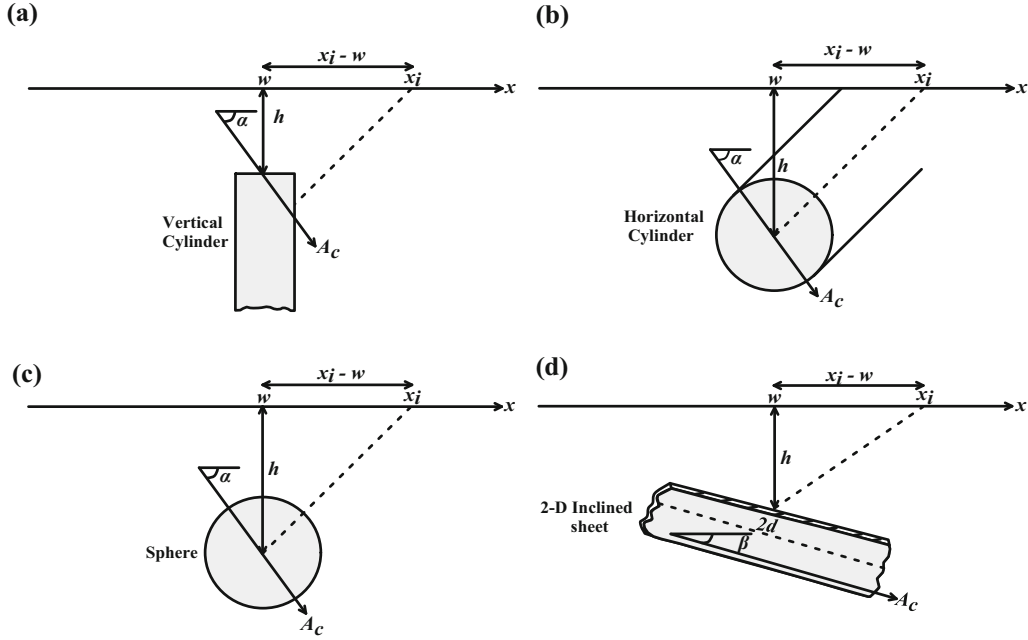


Fig. 1. Geometric structures for different simple bodies: **a** vertical cylinder, **b** horizontal cylinder, **c** sphere, and **d** 2-D inclined sheet.

Inversion Algorithm

The inversion algorithm applied in this study is based on the global PSO technique, which was proposed by Eberhart and Kennedy (1995). The method was developed for utilization in the solution of different geophysical problems (Sen and Stoffa 2013; Singh and Biswas 2016; Essa and Elhussein 2018, 2020; Essa 2019). The PSO technique is stochastic and, in this context, it can be used to represent a group of birds or school of fish looking for food. In this study, the models or particles represent the birds. Each model has a position and velocity vector, with the position vector representing the parameter value. A swarm is initiated with random models using the ranges of different variables, followed by updating the location and velocity of the different particles using the following formulas:

$$x_i^{k+1} = x_i^k + V_i^{k+1}, \quad (5)$$

where x_i^k is the i th particle position at the k th iteration, and V_i^k is the i th particle velocity at k th iteration and is obtained as follows:

$$V_i^{k+1} = c_3 V_i^k + c_1 \text{rand1}(T_{\text{best}} - x_i^{k+1}) + c_2 \text{rand2}(J_{\text{best}} - x_i^{k+1}), \quad (6)$$

where rand1 and rand2 are any two random values in the range [0,1], c_1 and c_2 are cognitive and social coefficients, c_3 is the inertial factor that controls the velocity of the model and takes on a value of < 1 , T_{best} is the best position reached by an individual model, and J_{best} is the global best position achieved by any model in the swarm. The c_1 and c_2 are usually equal to two (Parsopoulos and Vrahatis 2002; Singh and Biswas 2016; Essa 2019; Essa and Elhussein 2020). Then, the best solution reached by each individual model (T_{best}) and the global best solution reached (J_{best}) are stored in memory, and the location and velocity of the models are updated during the iteration process. The iteration process terminates when convergence is reached (Venter and Sobieski 2002; Essa and Elhussein 2020).

The global best solution (J_{best}) is reached when the following objective function (ψ_{obj}) is optimized:

$$\psi_{\text{obj}} = \frac{1}{M} \sum_{i=1}^M [V_{\text{resi}}^O(x_i) - V_{\text{resi}}^c(x_i)]^2, \quad (7)$$

where M is number of data points, V_{resi}^O is the observed self-potential anomaly, and V_{resi}^c is the calculated self-potential anomaly.

The different source parameters ($A_c, h, \alpha, \beta, d, S_f$, and w) were estimated by minimizing

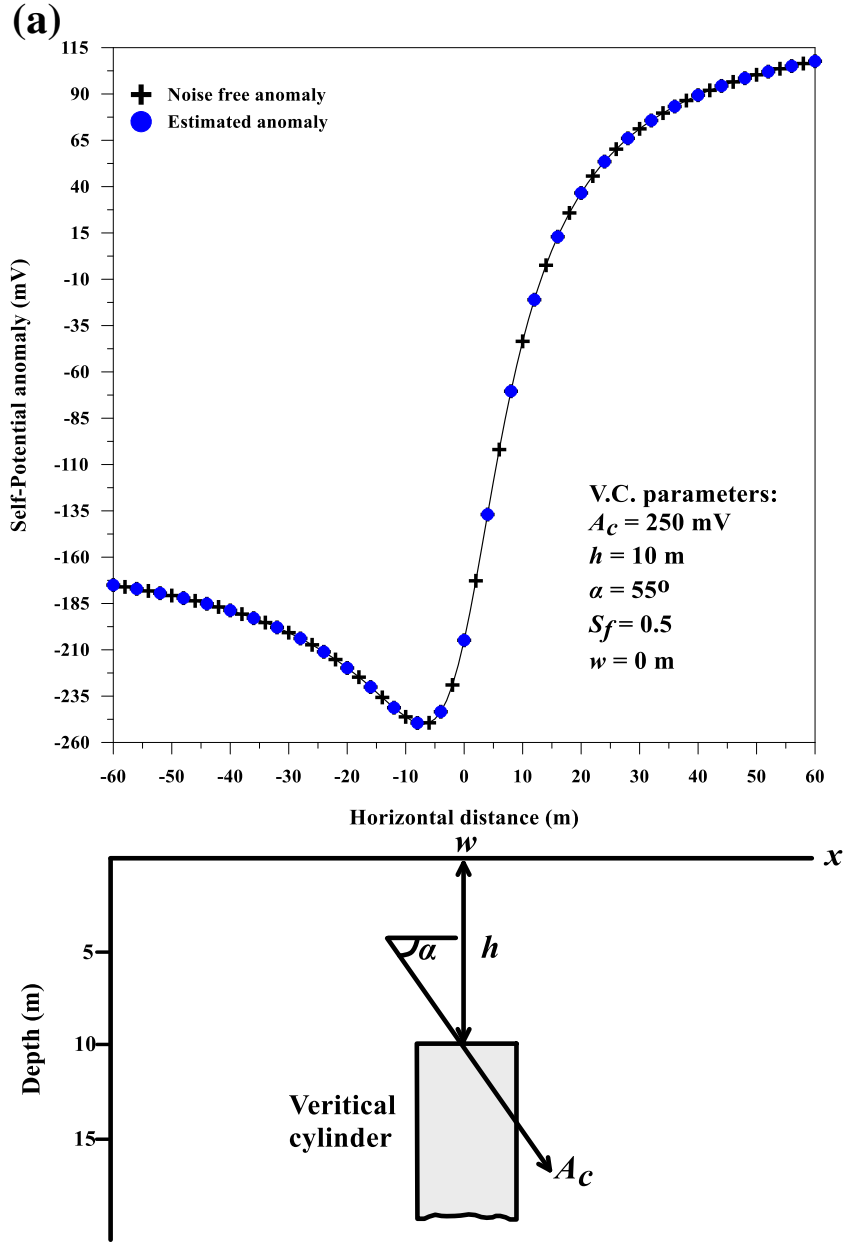


Fig. 2. **a** Synthetic noise-free self-potential anomaly from the vertical cylinder model with the following parameters: $A_c = 250$ mV, $h = 10$ m, $\alpha = 55^\circ$, $S_f = 0.5$, $w = 0$ m, and profile length = 120 m. The estimated anomaly is also presented. **b** First horizontal gradient anomalies of the self-potential anomaly in **a**. **c** Self-potential anomaly in **a** with 15% random noise and the estimated anomaly. **d** First horizontal gradient anomalies of the noisy self-potential anomaly in **c**.

Eq. (7) for the different s (window length) values used in Eq. (4). Then, the average value (\mathcal{E}) of the estimated parameters for the different s values was calculated. Finally, the root-mean-square (RMS) error was calculated as follows:

$$\text{RMS} = \sqrt{\frac{1}{M} \sum_{i=1}^M [V_{\text{resi}}^O(x_i) - V_{\text{resi}}^c(x_i)]^2}. \quad (8)$$

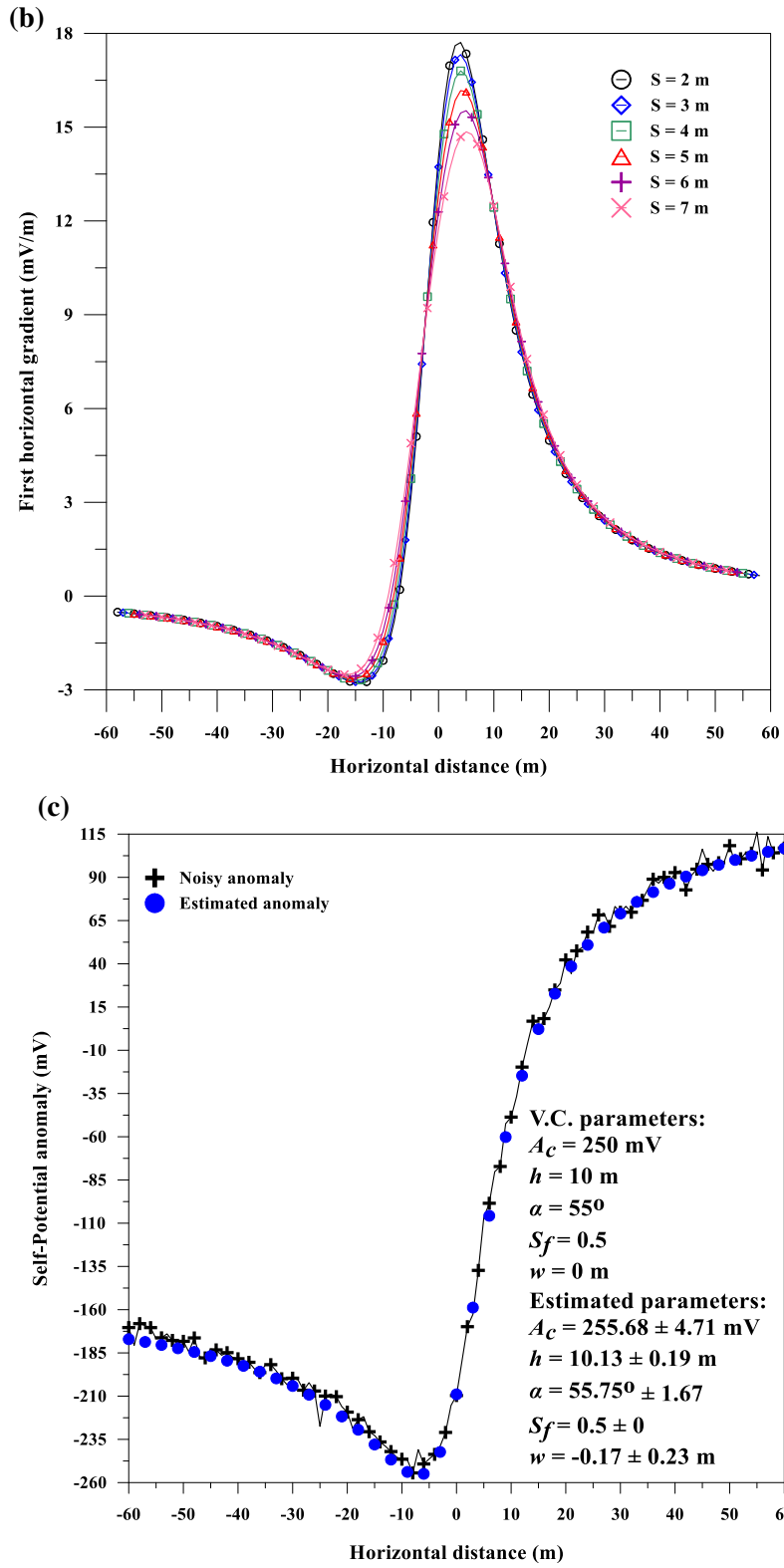


Fig. 2. continued.

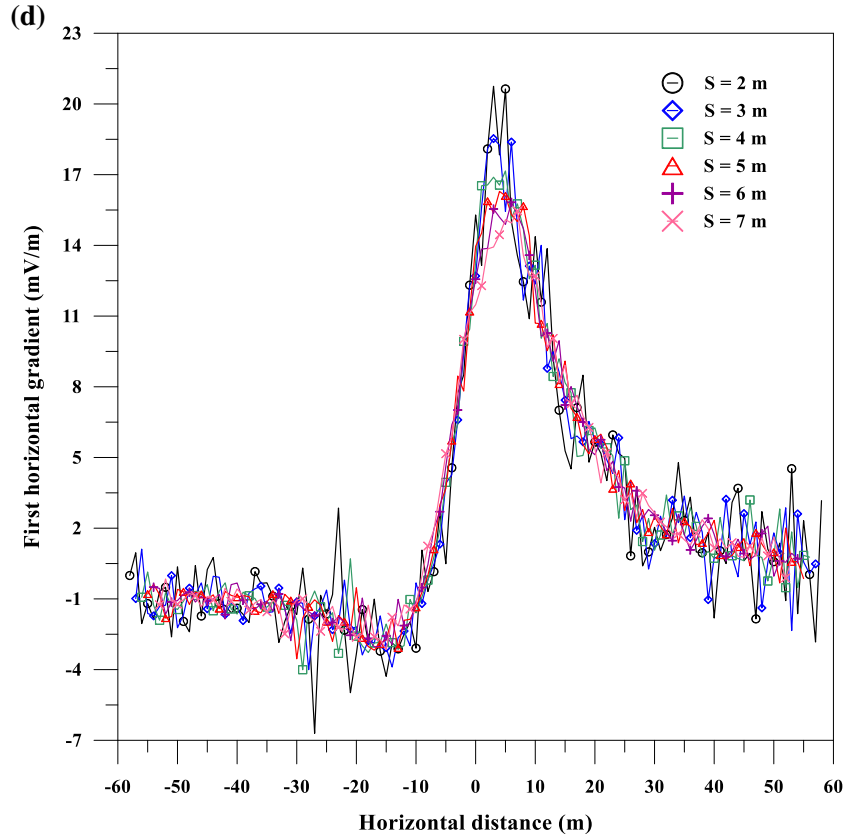


Fig. 2. continued.

Table 1. Numerical results of the global PSO inversion algorithm applied to first horizontal gradient anomalies from the vertical cylinder model ($A_c = 250$ mV, $h = 10$ m, $\alpha = 55^\circ$, $S_f = 0.5$, $w = 0$ m, profile length = 120 m), with and without 15% random noise

Parameters	Used range	$s = 2$ m	$s = 3$ m	$s = 4$ m	$s = 5$ m	$s = 6$ m	$s = 7$ m	\mathcal{E}	Error (%)	RMS error (mV)
Results (without noise)										
A_c (mV)	50–700	250	250	250	250	250	250	250 ± 0	0	0
h (m)	3–30	10	10	10	10	10	10	10 ± 0	0	
α (degree)	20–80	55	55	55	55	55	55	55 ± 0	0	
S_f (dimensionless)	0.2–2	0.5	0.5	0.5	0.5	0.5	0.5	0.5 ± 0	0	
w (m)	– 10–10	0	0	0	0	0	0	0 ± 0	–	
Results (using 15% random noise)										
A_c (mV)	50–700	255.40	253.80	257.00	247.70	258.90	261.30	255.68 ± 4.71	2.27	5.82
h (m)	3–30	10.30	10.00	10.30	9.90	10.00	10.30	10.13 ± 0.19	1.30	
α (degree)	20–80	58.22	57.00	54.00	56.06	55.13	54.09	55.75 ± 1.67	1.36	
S_f (dimensionless)	0.2–2	0.50	0.50	0.50	0.50	0.50	0.50	0.50 ± 0.00	0.00	
w (m)	– 10–10	– 0.41	– 0.34	0.07	– 0.36	– 0.06	0.10	$– 0.17 \pm 0.23$	–	

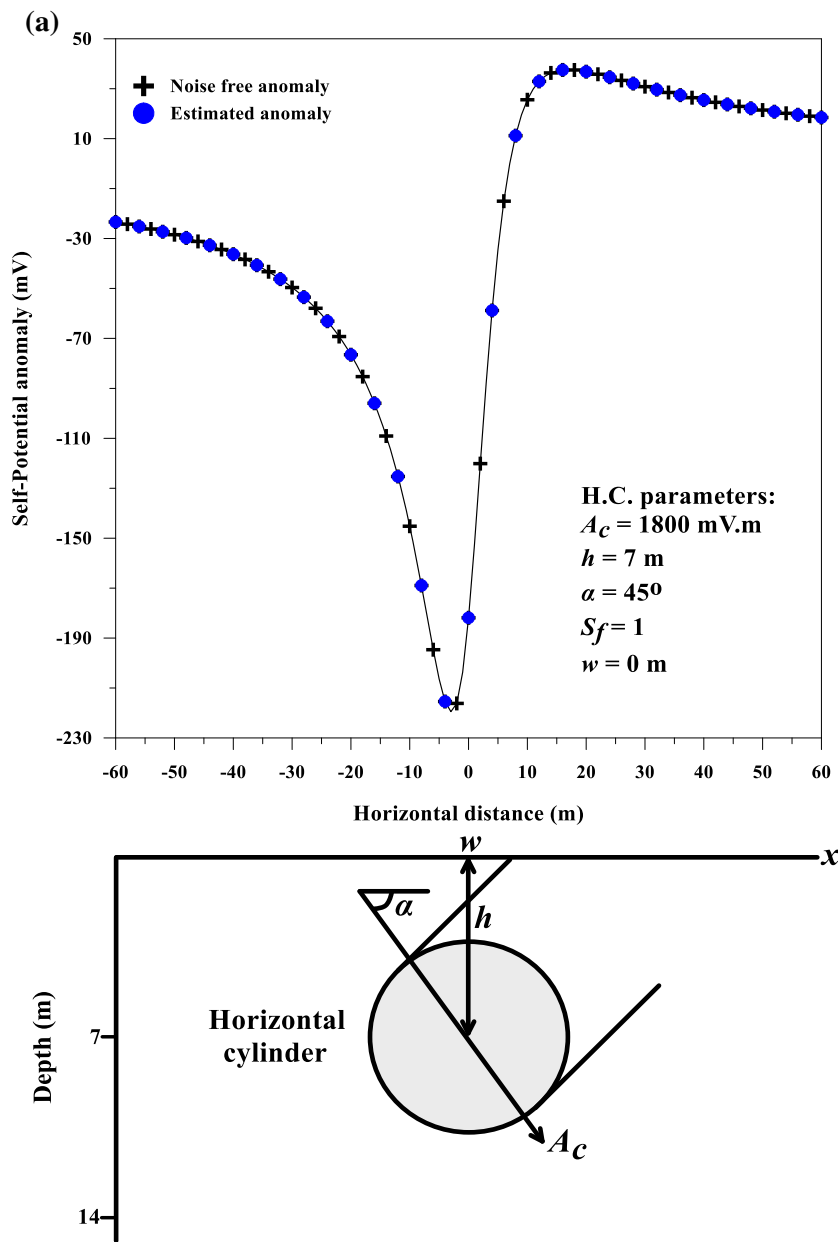


Fig. 3. **a** Synthetic noise-free self-potential anomaly from the horizontal cylinder model with the following parameters: $A_c = 1800 \text{ mV}\cdot\text{m}$, $h = 7 \text{ m}$, $\alpha = 45^\circ$, $S_f = 1$, $w = 0 \text{ m}$, and profile length = 120 m. The estimated anomaly is also presented. **b** First horizontal gradient anomalies of the self-potential anomaly in **a**. **c** Self-potential anomaly in **a** with 15% random noise and the estimated anomaly. **d** First horizontal gradient anomalies of the noisy self-potential anomaly in **c**.

SYNTHETIC MODELS

In these models, the proposed method was applied to five synthetic examples representing differ-

ent sources (semi-infinite vertical cylinder, horizontal cylinder, sphere, and 2-D inclined sheet) contaminated with and without 15% random noise. One of these examples includes a regional background to determine the effect of the background on the proposed method.

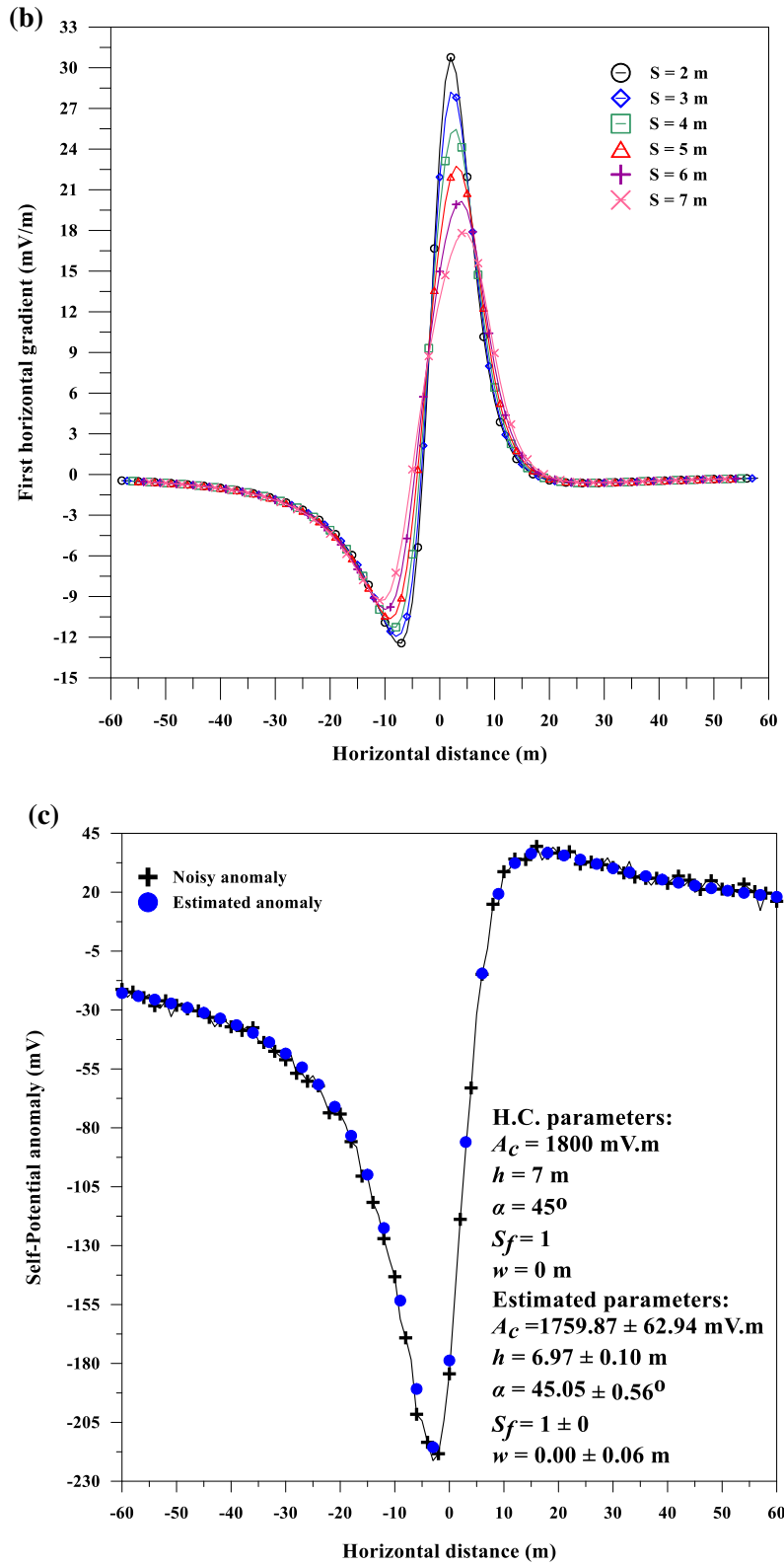


Fig. 3. continued.

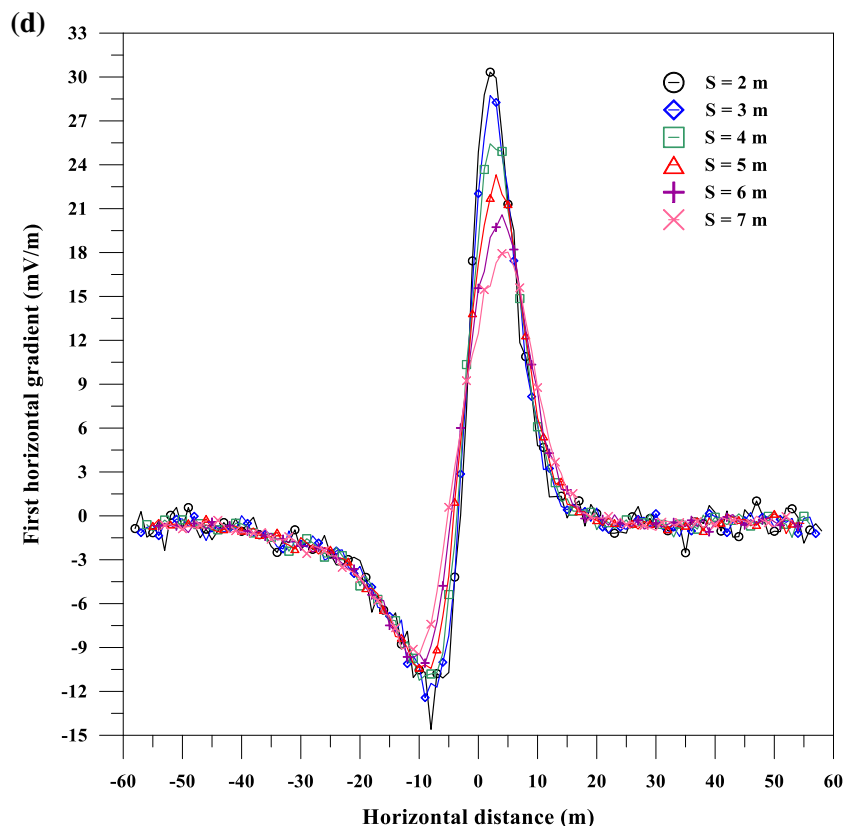


Fig. 3. continued.

Table 2. Numerical results of the global PSO inversion algorithm applied to first horizontal gradient anomalies from the horizontal cylinder model ($A_c = 1800$ mV m, $h = 7$ m, $\alpha = 45^\circ$, $S_f = 1$, $w = 0$ m, profile length = 120 m), with and without 15% random noise

Parameters	Used range	$s = 2$ m	$s = 3$ m	$s = 4$ m	$s = 5$ m	$s = 6$ m	$s = 7$ m	\mathcal{E}	Error (%)	RMS error (mV)
Results (without noise)										
A_c (mV.m)	800–2800	1800	1800	1800	1800	1800	1800	1800 ± 0	0	0
h (m)	3–30	7	7	7	7	7	7	7 ± 0	0	
α (degree)	20–80	45	45	45	45	45	45	45 ± 0	0	
S_f (dimensionless)	0.2–2	1	1	1	1	1	1	1 ± 0	0	
w (m)	– 10–10	0	0	0	0	0	0	0 ± 0	–	
Results (with 15% random noise)										
A_c (mV.m)	800–2800	1762.30	1685.70	1858.20	1784.90	1697.50	1770.60	1759.87 ± 62.94	2.23	2.85
h (m)	3–30	7.10	7.00	6.80	7.00	7.00	6.90	6.97 ± 0.10	0.43	
α (degree)	20–80	45.50	44.15	45.30	45.26	44.57	45.53	45.05 ± 0.56	0.11	
S_f (dimensionless)	0.2–2	1.00	1.00	1.00	1.00	1.00	1.00	1.00 ± 0.00	0.00	
w (m)	– 10–10	– 0.06	0.09	0.05	– 0.03	0.00	– 0.04	0.00 ± 0.06	–	

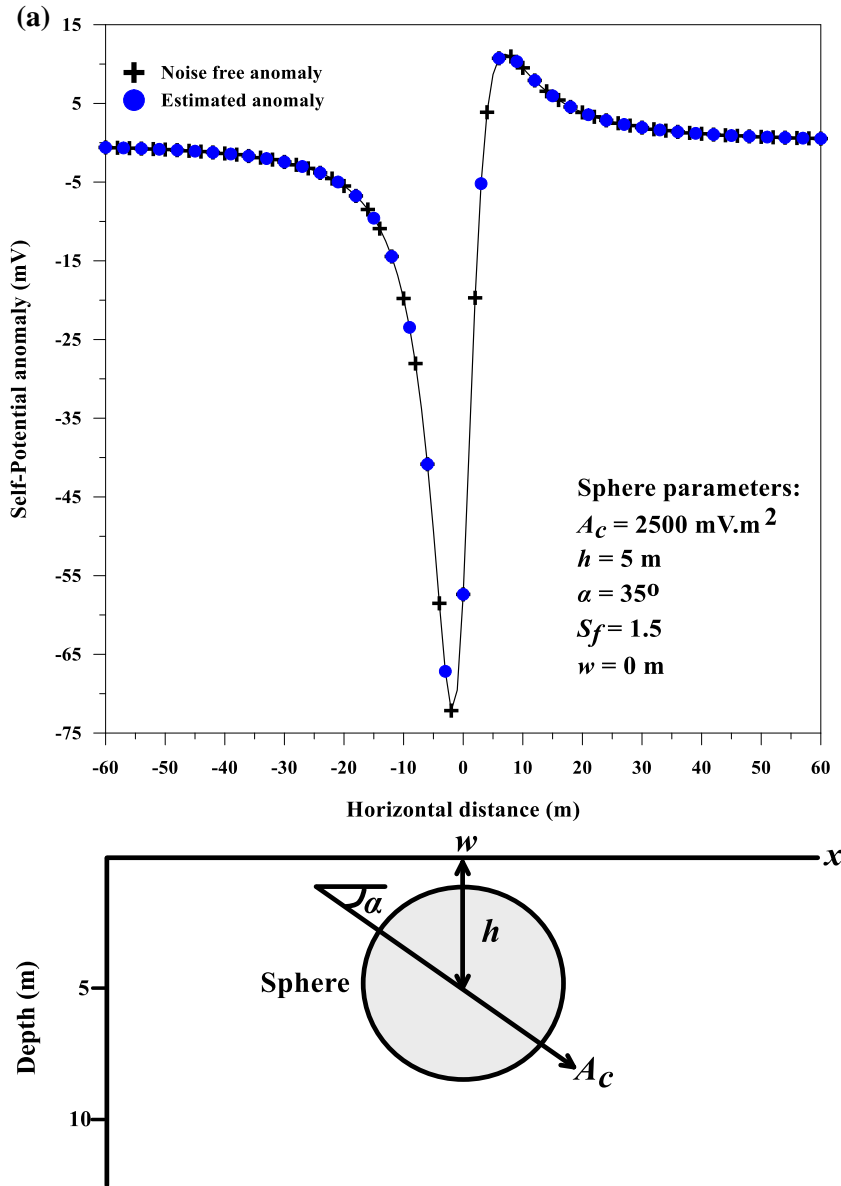


Fig. 4. **a** Synthetic noise-free self-potential anomaly from the sphere model with the following parameters: $A_c = 2500 \text{ mV}\cdot\text{m}^2$, $h = 5 \text{ m}$, $\alpha = 35^\circ$, $S_f = 1.5$, $w = 0 \text{ m}$, and profile length = 120 m. The estimated anomaly is also presented. **b** First horizontal gradient anomalies of the self-potential anomaly in **a**. **c** Self-potential anomaly mentioned in **a** with 15% random noise and the estimated anomaly. **d** First horizontal gradient anomalies of the noisy self-potential anomaly in **c**.

Semi-Infinite Vertical Cylinder Example

A pure self-potential anomaly from a semi-infinite vertical cylinder was calculated using profile length = 120 m, $A_c = 250 \text{ mV}$, $h = 10 \text{ m}$, $\alpha = 55^\circ$, S_f

= 0.5, and $w = 0 \text{ m}$ (Fig. 2a). The first horizontal gradient was then applied to the self-potential anomaly profile using different s values ($s = 2, 3, 4, 5, 6,$ and 7 m) (Fig. 2b), and the global PSO technique was applied to these gradient anomalies to estimate the vertical cylinder model parameters

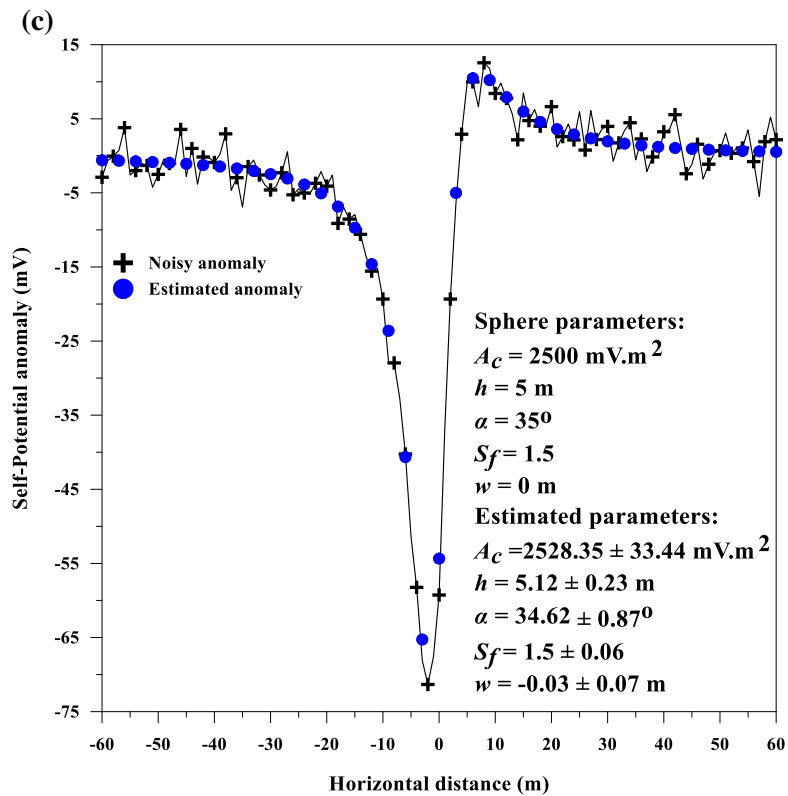
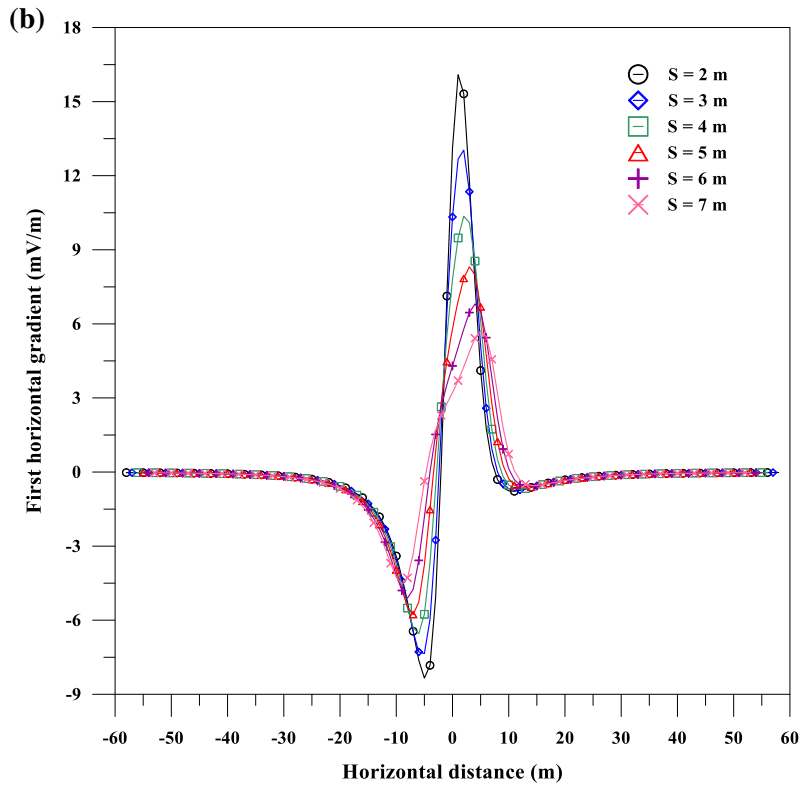


Fig. 4. continued.

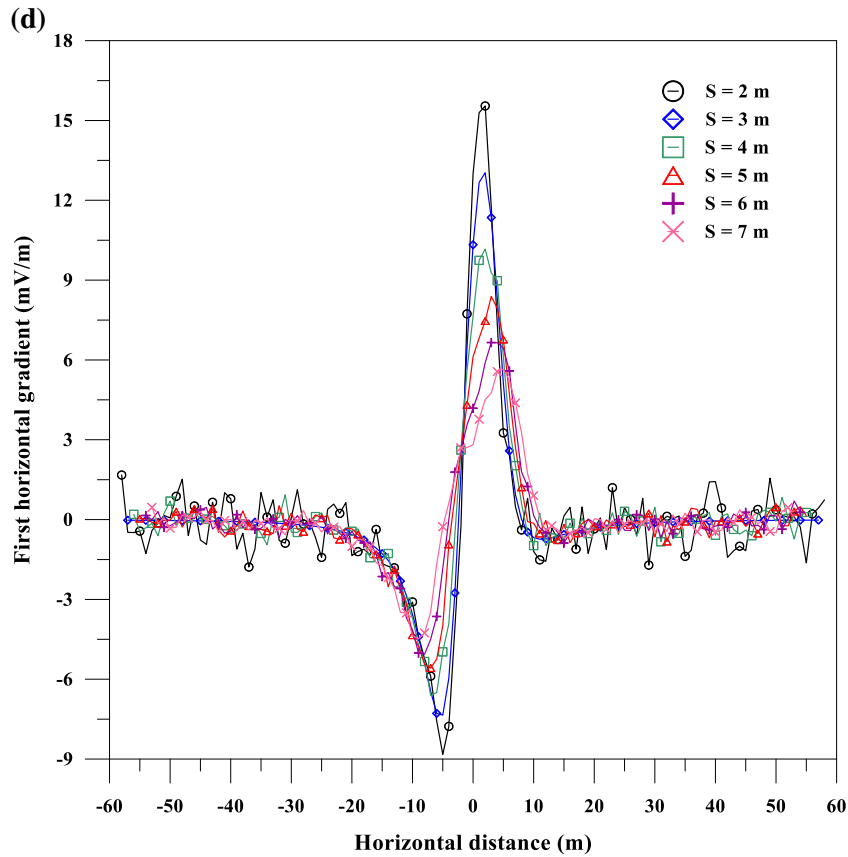


Fig. 4. continued.

Table 3. Numerical results of the global PSO inversion algorithm applied to first horizontal gradient anomalies from the sphere model ($A_c = 2500 \text{ mV m}^2$, $h = 5 \text{ m}$, $\alpha = 35^\circ$, $S_f = 1.5$, $w = 0 \text{ m}$, profile length = 120 m), with and without 15% random noise

Parameters	Used range	$s = 2 \text{ m}$	$s = 3 \text{ m}$	$s = 4 \text{ m}$	$s = 5 \text{ m}$	$s = 6 \text{ m}$	$s = 7 \text{ m}$	\mathcal{E}	Error (%)	RMS error (mV)
Results (without noise)										
$A_c \text{ (mV m}^2\text{)}$	1000–3500	2500	2500	2500	2500	2500	2500	2500 ± 0	0	0
$h \text{ (m)}$	2–30	5	5	5	5	5	5	5 ± 0	0	
$\alpha \text{ (degree)}$	20–70	35	35	35	35	35	35	35 ± 0	0	
$S_f \text{ (dimensionless)}$	0.2–2	1.5	1.5	1.5	1.5	1.5	1.5	1.5 ± 0	0	
$w \text{ (m)}$	–10–10	0	0	0	0	0	0	0 ± 0	–	
Results (with 15% random noise)										
$A_c \text{ (mV m}^2\text{)}$	1000–3500	2578.00	2486.40	2525.70	2545.90	2497.10	2537.00	2528.35 ± 33.44	1.13	2.19
$h \text{ (m)}$	2–30	4.80	5.10	5.50	5.00	5.20	5.10	5.12 ± 0.23	2.40	
$\alpha \text{ (degree)}$	20–70	35.05	35.50	33.70	35.28	34.80	33.40	34.62 ± 0.87	1.09	
$S_f \text{ (dimensionless)}$	0.2–2	1.40	1.50	1.50	1.50	1.60	1.50	1.50 ± 0.06	0.00	
$w \text{ (m)}$	–10–10	–0.04	–0.01	0.08	–0.02	–0.12	–0.06	$–0.03 \pm 0.07$	–	

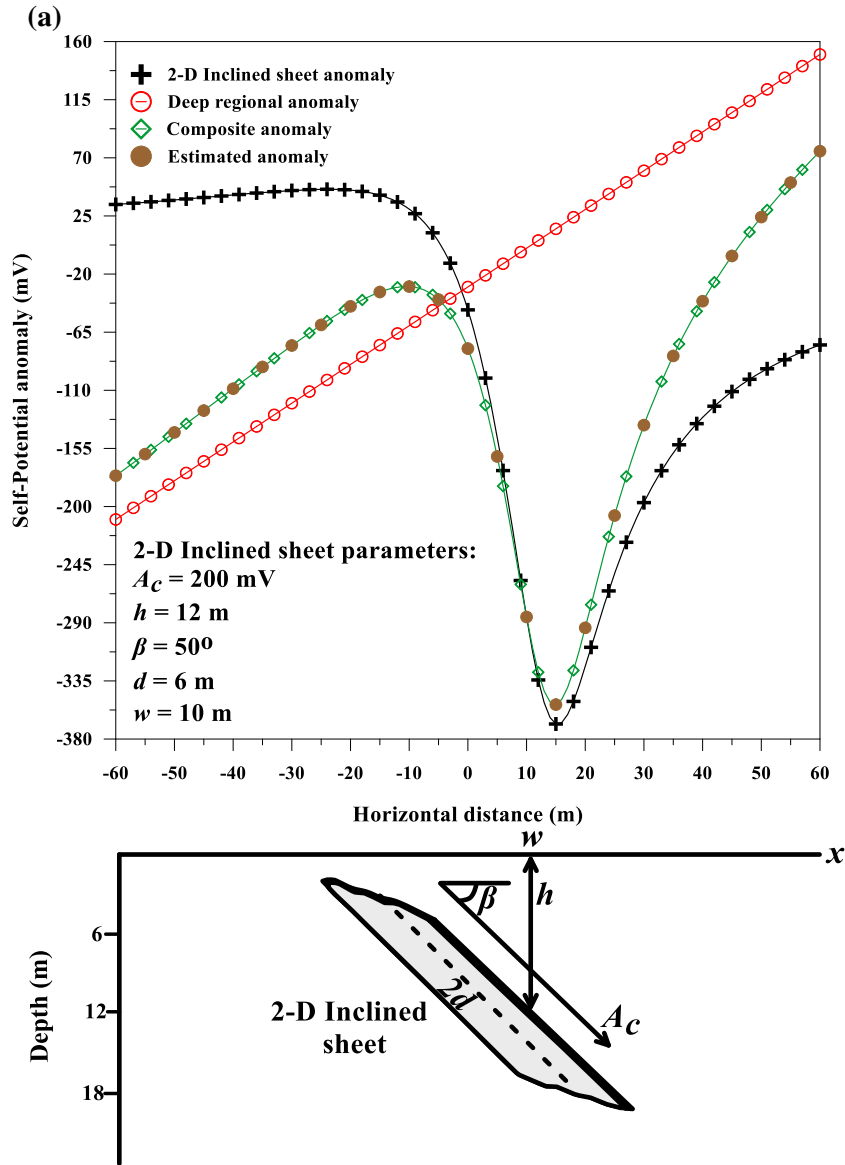


Fig. 5. a Noise-free composite synthetic self-potential anomaly of a 2-D inclined sheet model with the following parameters; $A_c = 200$ mV, $h = 12$ m, $\beta = 50^\circ$, $d = 6$ m, $w = 10$ m, profile length = 120 m, and deep-seated first-order regional anomaly ($3x_i - 30$). The estimated anomaly is also presented. **b** First horizontal gradient anomalies of the composite self-potential anomaly in **a**. **c** Composite self-potential anomaly mentioned in **a** with 15% random noise and the estimated anomaly. **d** First horizontal gradient anomalies of the noisy composite self-potential anomaly in **c**.

using different ranges per parameter (Table 1). Table 1 shows the estimated parameters (A_c , h , α , S_f , and w), where the errors of A_c , h , α , and S_f were 0% and the RMS error was 0 mV. The correlation between the noise-free anomaly and estimated anomaly is shown in Fig. 2a.

To test the efficiency of the proposed method in the case of noisy data, the previous synthetic model was contaminated with 15% random noise (Fig. 2c). The first horizontal gradient anomalies were calculated using the same previous window lengths ($s = 2, 3, 4, 5, 6, \text{ and } 7$ m) (Fig. 2d); then, by applying the PSO

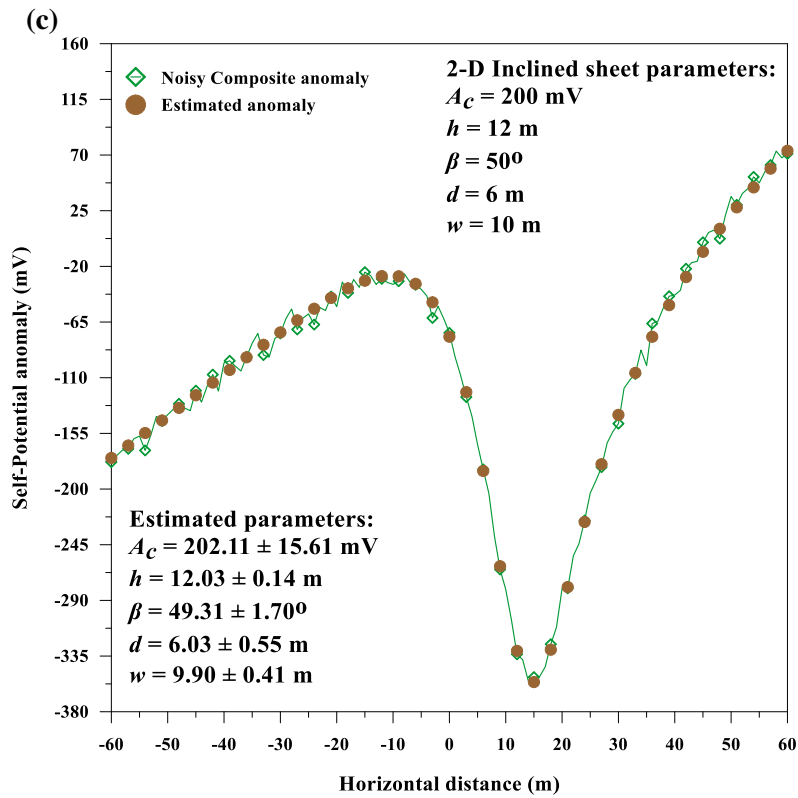
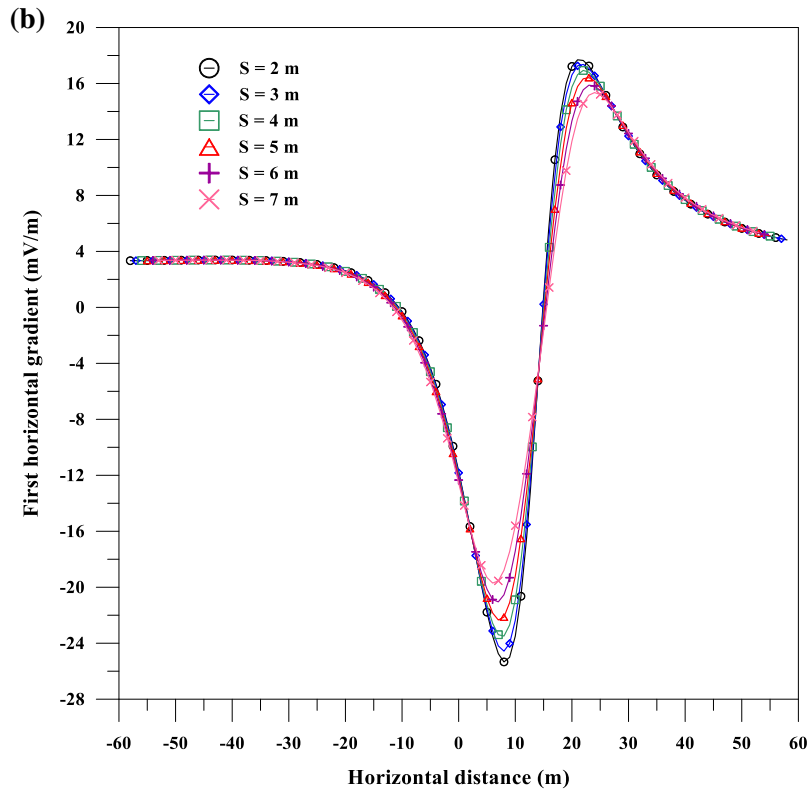


Fig. 5. continued.

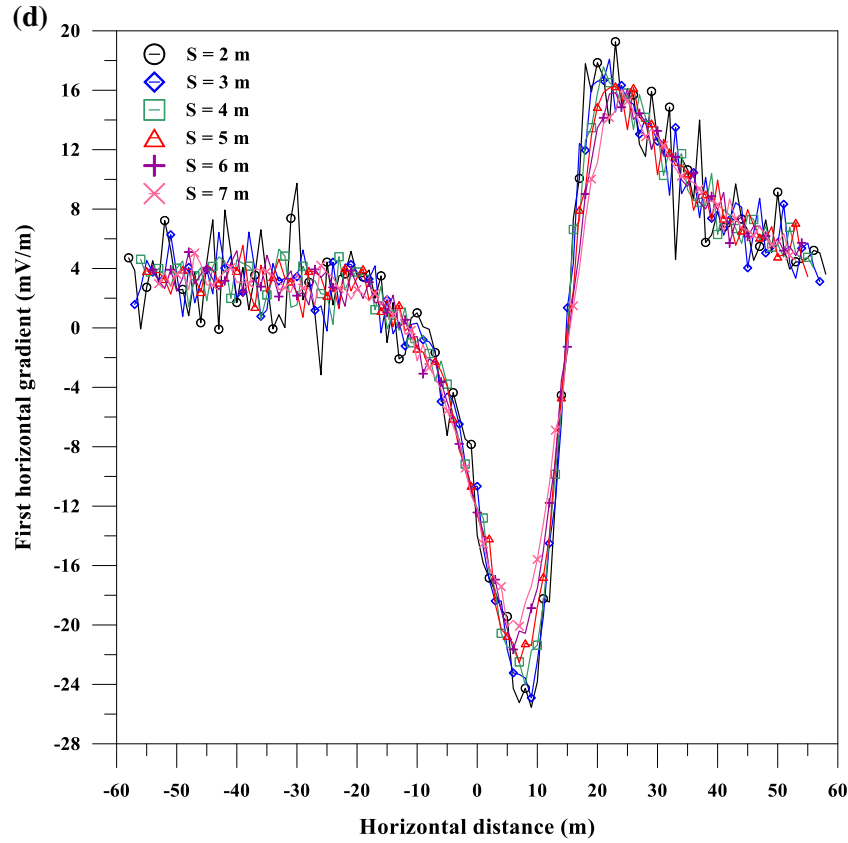


Fig. 5. continued.

Table 4. Numerical results of the global PSO inversion algorithm applied to first horizontal gradient anomalies from the composite anomaly of 2-D inclined sheet ($A_c = 200$ mV, $h = 12$ m, $\beta = 50^\circ$, $d = 6$ m, $w = 10$ m, profile length = 120 m) and deep-seated first-order regional anomaly ($3x_i - 30$), with and without 15% random noise

Parameters	Used range	$s = 2$ m	$s = 3$ m	$s = 4$ m	$s = 5$ m	$s = 6$ m	$s = 7$ m	\mathcal{E}	Error (%)	RMS error (mV)
Results (without noise)										
A_c (mV)	50–750	200	200	200	200	200	200	200 ± 0	0	0
h (m)	2–30	12	12	12	12	12	12	12 ± 0	0	
β (degree)	20–80	50	50	50	50	50	50	50 ± 0	0	
d (m)	2–20	6	6	6	6	6	6	6 ± 0	0	
w (m)	– 10–30	10	10	10	10	10	10	10 ± 0	0	
Results (with 15% random noise)										
A_c (mV)	50–750	218.55	198.96	173.82	202.21	213.20	205.93	202.11 ± 15.61	1.06	6.13
h (m)	2–30	11.80	12.20	12.00	12.10	12.00	12.10	12.03 ± 0.14	0.25	
β (degree)	20–80	50.51	48.07	46.41	49.87	50.50	50.49	49.31 ± 1.70	1.38	
d (m)	2–20	5.40	6.20	7.00	6.00	5.70	5.90	6.03 ± 0.55	0.50	
w (m)	– 10–30	10.35	9.78	9.17	9.86	10.17	10.08	9.90 ± 0.41	1.00	

method to the gradient anomalies, the different parameters were estimated (Table 1). Table 1 shows the estimated parameters ($A_c = 255.68 \pm 4.71$ mV,

$h = 10.13 \pm 0.19$ m, $\alpha = 55.75 \pm 1.67^\circ$, $S_f = 0.5 \pm 0$, and $w = -0.17 \pm 0.23$ m), where the errors of A_c , h , α , and S_f were 2.27%, 1.30%, 1.36%, and 0%

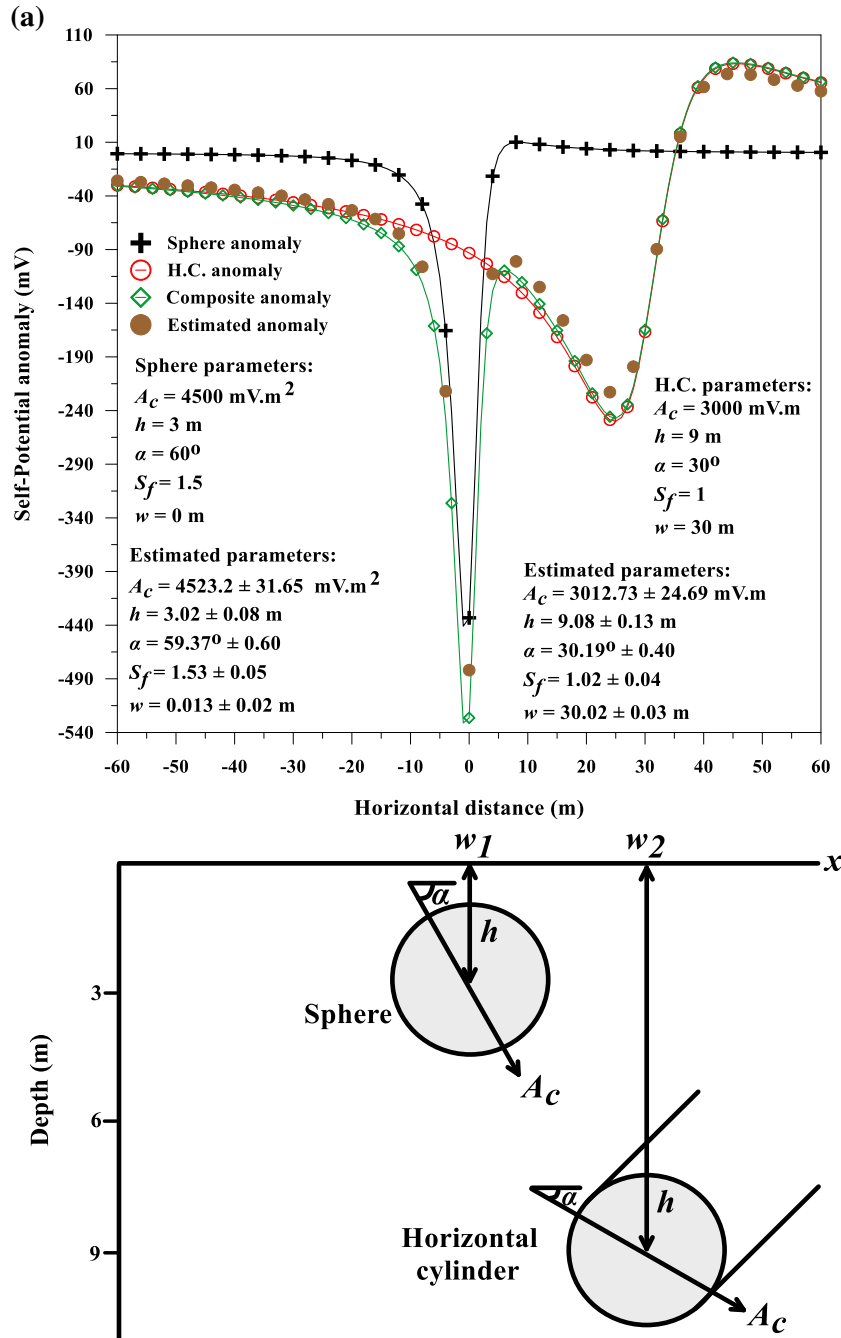


Fig. 6. a Noise-free composite multi-model anomaly of the sphere ($A_c = 4500 \text{ mV}\cdot\text{m}^2$, $h = 3 \text{ m}$, $\alpha = 60^\circ$, $S_f = 1.5$ m, and $w = 0 \text{ m}$). and horizontal cylinder ($A_c = 3000 \text{ mV}\cdot\text{m}$, $h = 9 \text{ m}$, $\alpha = 30^\circ$, $S_f = 1$ m, and $w = 30 \text{ m}$). using a profile length of 120 m. The estimated anomaly is also presented. **b** First horizontal gradient anomalies of the composite self-potential anomaly in **a**. **c** Composite self-potential anomaly mentioned in **a** with 15% random noise and the estimated anomaly. **d** First horizontal gradient anomalies of the noisy composite self-potential anomaly in **c**.

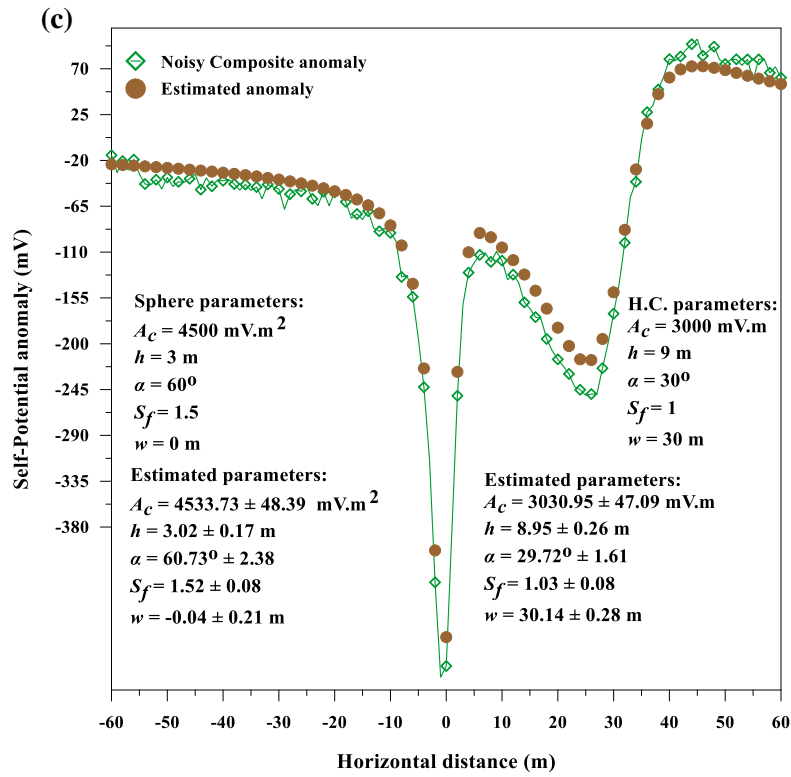
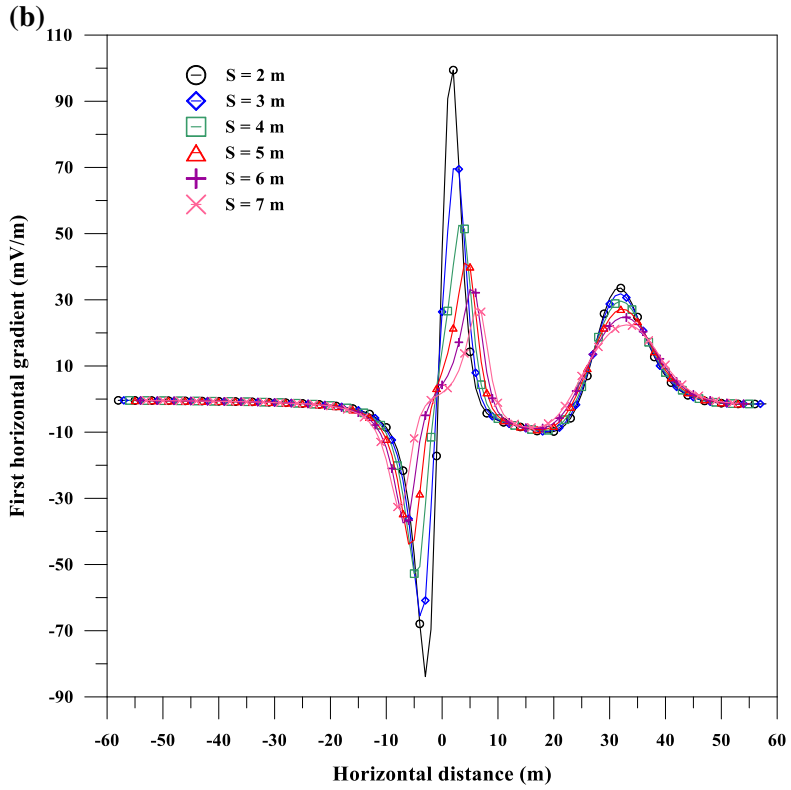


Fig. 6. continued.

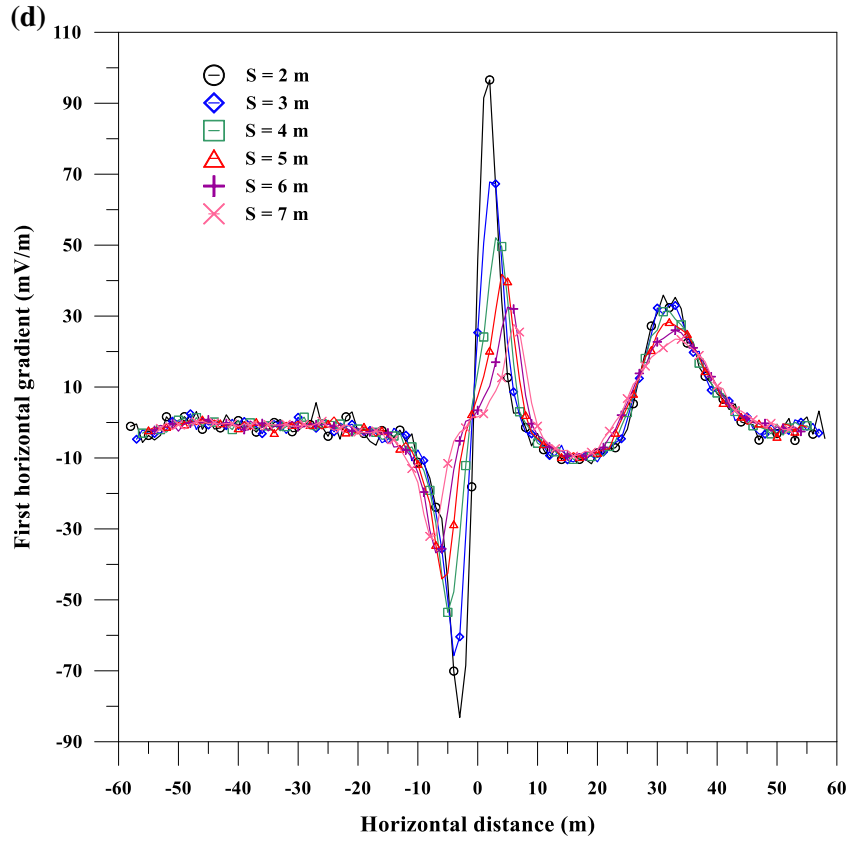


Fig. 6. continued.

respectively, and the RMS error was 5.82 mV. Figure 2c compares the noisy and calculated anomalies.

Horizontal Cylinder Example

A noise-free self-potential anomaly from a horizontal cylinder was calculated using: profile length = 120 m, $A_c = 1800$ mV m, $h = 7$ m, $\alpha = 45^\circ$, $S_f = 1$, and $w = 0$ m (Fig. 3a). The first horizontal gradient was then applied to the self-potential anomaly profile using different s values ($s = 2, 3, 4, 5, 6,$ and 7 m) (Fig. 3b); then, the global PSO technique was applied to these gradient anomalies to estimate the horizontal cylinder model parameters using different ranges per parameter (Table 2). Table 2 shows the estimated parameters ($A_c, h, \alpha, S_f,$ and w), where the errors of $A_c, h, \alpha,$ and S_f were 0% and the RMS error was 0 mV.

To apply the proposed method to noisy data, as most real data include noise, the previous synthetic

model was contaminated with 15% random noise (Fig. 3c). The first horizontal gradient anomalies were calculated using the same previous window lengths ($s = 2, 3, 4, 5, 6,$ and 7 m) (Fig. 3d); then, by applying the PSO method to the gradient anomalies, the different parameters were estimated (Table 2). Table 2 shows the estimated parameters ($A_c = 1759.87 \pm 62.94$ mV m, $h = 6.97 \pm 0.10$ m, $\alpha = 45.05 \pm 0.56^\circ$, $S_f = 1 \pm 0$, and $w = 0.00 \pm 0.06$ m), where the errors of $A_c, h, \alpha,$ and S_f were 2.23%, 0.43%, 0.11%, and 0%, respectively, and the RMS error was 2.85 mV. Figure 3c compares the noisy and calculated anomalies.

Sphere Example

A pure self-potential anomaly from a sphere was calculated using: profile length = 120 m, $A_c = 2500$ mV m², $h = 5$ m, $\alpha = 35^\circ$, $S_f = 1.5$, and $w = 0$ m (Fig. 4a). The first horizontal gradient was

Table 5. Results of the global PSO inversion algorithm applied to first horizontal gradient anomalies from the composite multi-model anomaly of sphere ($A_c = 4500 \text{ mV}\cdot\text{m}^2$, $h = 3 \text{ m}$, $\alpha = 60^\circ$, $S_f = 1.5 \text{ m}$, $w = 0 \text{ m}$, profile length = 120 m) and horizontal cylinder ($A_c = 3000 \text{ mV m}$, $h = 9 \text{ m}$, $\alpha = 30^\circ$, $S_f = 1 \text{ m}$, $w = 30 \text{ m}$, profile length = 120 m), with and without 15% random noise

Model	Parameters	Used ranges	$s = 2 \text{ m}$	$s = 3 \text{ m}$	$s = 4 \text{ m}$	$s = 5 \text{ m}$	$s = 6 \text{ m}$	$s = 7 \text{ m}$	\mathcal{E}	Error (%)	RMS error (mV)
Results (without noise)											
Sphere	$A_c \text{ (mV m}^2\text{)}$	2000–6000	4550.50	4500.00	4482.20	4565.80	4530.70	4510.00	4523.20 ± 31.65	0.52	14.43
	$h \text{ (m)}$	1–25	3.10	3.00	2.90	3.00	3.10	3.00	3.02 ± 0.08	0.67	
	$\alpha \text{ (}^\circ\text{)}$	20–80	59.00	59.06	60.00	58.52	60.00	59.61	59.37 ± 0.60	1.05	
	$S_f \text{ (dimensionless)}$	0.2–2	1.50	1.60	1.50	1.50	1.60	1.50	1.53 ± 0.05	2.00	
	$w \text{ (m)}$	– 10–10	0.04	0.01	– 0.02	0.03	0.00	0.02	0.013 ± 0.02	–	
Horizontal cylinder	$A_c \text{ (mV m)}$	1500–5000	3020.40	2979.90	3000.00	3025.70	3000.00	3050.40	3012.73 ± 24.69	0.42	
	$h \text{ (m)}$	1–25	9.00	9.00	9.20	9.00	9.30	9.00	9.08 ± 0.13	0.8	
	$\alpha \text{ (}^\circ\text{)}$	20–80	30.07	30.00	30.09	30.00	30.00	31.00	30.19 ± 0.40	0.63	
	$S_f \text{ (dimensionless)}$	0.2–2	1.00	1.00	1.00	1.10	1.00	1.00	1.02 ± 0.04	2.00	
	$w \text{ (m)}$	10–50	30.00	30.00	30.05	30.00	30.00	30.06	30.02 ± 0.03	0.07	
Results (with 15% random noise)											
Sphere	$A_c \text{ (mV m}^2\text{)}$	2000–6000	4474.20	4495.80	4550.10	4573.40	4509.60	4599.30	4533.73 ± 48.39	0.75	17.85
	$h \text{ (m)}$	1–25	2.90	3.00	3.30	3.00	3.10	2.80	3.02 ± 0.17	0.67	
	$\alpha \text{ (}^\circ\text{)}$	20–80	57.28	62.90	58.94	60.00	62.02	63.23	60.73 ± 2.38	1.22	
	$S_f \text{ (dimensionless)}$	0.2–2	1.50	1.60	1.40	1.50	1.50	1.60	1.52 ± 0.08	1.33	
	$w \text{ (m)}$	– 10–10	– 0.01	– 0.27	0.08	0.29	– 0.21	– 0.12	$– 0.04 \pm 0.21$	–	
Horizontal cylinder	$A_c \text{ (mV m)}$	1500–5000	3010.40	2975.60	2991.30	3079.20	3091.40	3037.80	3030.95 ± 47.09	1.03	
	$h \text{ (m)}$	1–25	8.90	8.60	8.80	9.20	8.90	9.30	8.95 ± 0.26	0.56	
	$\alpha \text{ (}^\circ\text{)}$	20–80	28.90	32.15	29.40	28.79	31.17	27.91	29.72 ± 1.61	0.93	
	$S_f \text{ (dimensionless)}$	0.2–2	1.10	0.90	1.10	1.00	1.00	1.10	1.03 ± 0.08	3.00	
	$w \text{ (m)}$	10–50	30.24	29.58	30.15	30.35	30.33	30.17	30.14 ± 0.28	0.47	

then applied to the self-potential anomaly profile using different s values ($s = 2, 3, 4, 5, 6$, and 7 m) (Fig. 4b); then, the global PSO technique was applied to these gradient anomalies to estimate the sphere model parameters using different ranges per parameter (Table 3). Table 3 shows the estimated parameters (A_c, h, α, S_f , and w), where the errors of A_c, h, α , and S_f were 0% and the RMS error was 0 mV.

To examine the effect of noisy data on the proposed method, the previous synthetic model was contaminated with 15% random noise (Fig. 4c). The first horizontal gradient anomalies were calculated using the same previous window lengths ($s = 2, 3, 4, 5, 6$, and 7 m) (Fig. 4d); then, by applying the PSO method to the gradient anomalies, the different

parameters were estimated (Table 3). Table 3 shows the estimated parameters ($A_c = 2528.35 \pm 33.44 \text{ mV m}^2, h = 5.12 \pm 0.23 \text{ m}, \alpha = 34.62 \pm 0.87^\circ, S_f = 1.5 \pm 0.06$, and $w = -0.03 \pm 0.07 \text{ m}$), where the errors of A_c, h, α , and S_f were 1.13%, 2.4%, 1.09%, and 0%, respectively, and the RMS error was 2.19 mV. Figure 4c compared the noisy and calculated anomalies.

2-D Inclined Sheet Example with Regional Background

The efficiency of our method in the presence of a regional background was tested. To do so, a noise-free self-potential anomaly from a 2-D inclined

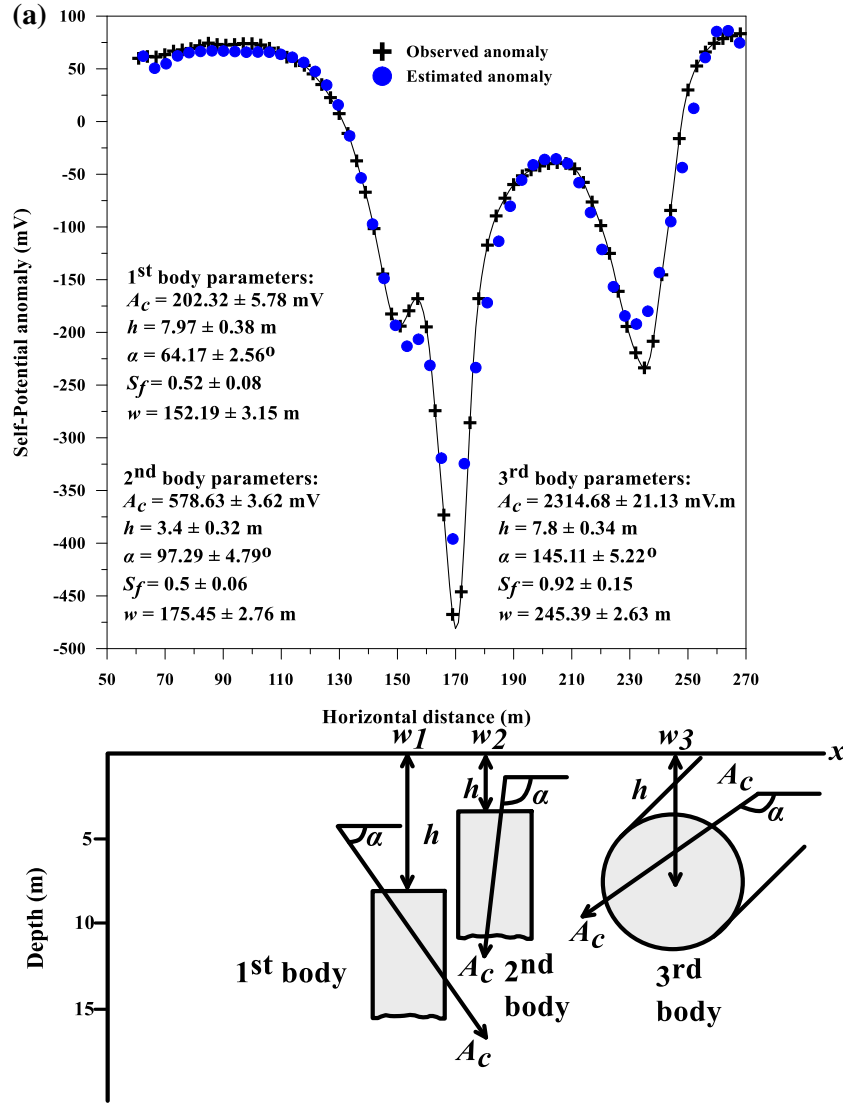


Fig. 7. Senneterre, Quebec, Canada: **a** Observed and the estimated self-potential anomaly profile for the multi-source field example of sulfide deposit, and the geometric structure of the three different sources. **b** First horizontal gradient anomalies of the observed self-potential anomaly in **a**.

sheet ($A_c = 200$ mV, $h = 12$ m, $\beta = 50^\circ$, $d = 6$ m, and $w = 10$ m) was added to a deep-seated first-order regional anomaly ($3x_i - 30$) (Fig. 5a) with a profile length of 120 m. The composite anomaly was obtained as follows:

$$\begin{aligned} \Delta V(x_i, h, \beta, d) &= 200 \ln \left[\frac{((x_i - 10) - 6 \cos 50^\circ)^2 + (12 - 6 \sin 50^\circ)^2}{((x_i - 10) + 6 \cos \beta)^2 + (12 + 6 \sin 50^\circ)^2} \right] \\ &+ (3x_i - 30), i = 0, 1, 2, 3, \dots, M \end{aligned} \tag{9}$$

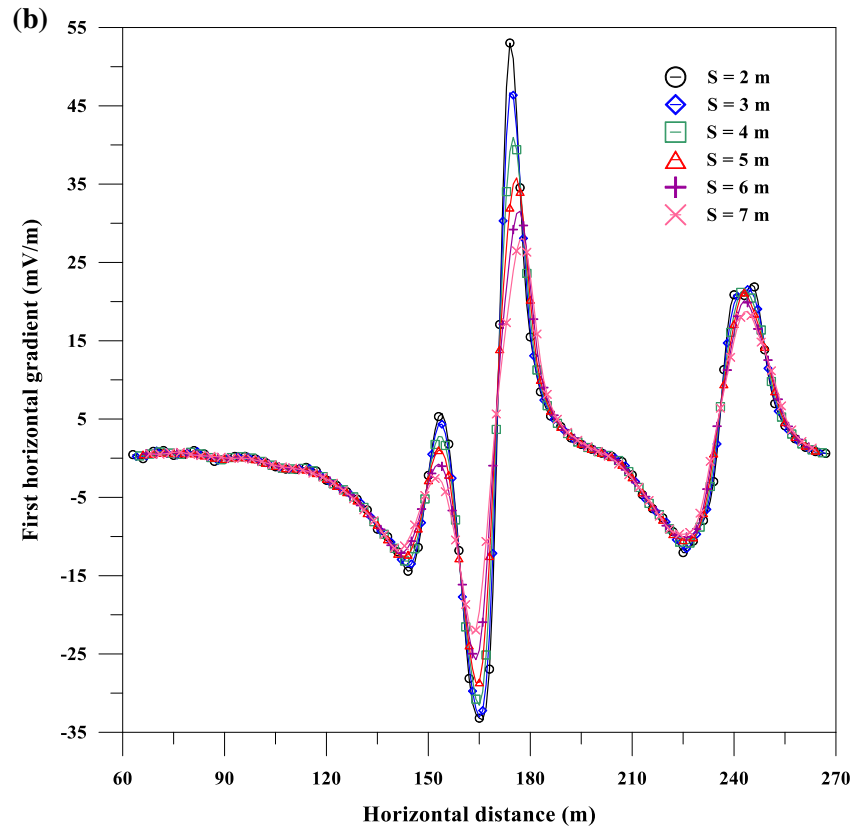


Fig. 7. continued.

Table 6. Results of the global PSO inversion algorithm applied to first horizontal gradient anomalies for the multi- source self-potential anomaly of sulfide deposit, Senneterre, Quebec, Canada

Model	Parameters	Used ranges	$s = 2 \text{ m}$	$s = 3 \text{ m}$	$s = 4 \text{ m}$	$s = 5 \text{ m}$	$s = 6 \text{ m}$	$s = 7 \text{ m}$	\mathcal{E}	RMS error (mV)
First body (anomaly)	A_c (mV)	100–1500	205.70	201.40	195.10	197.00	210.80	203.90	202.32 ± 5.78	24.01
	h (m)	0.5–80	8.10	7.80	8.00	7.30	8.40	8.20	7.97 ± 0.38	
	α ($^\circ$)	0–180	67.00	63.00	67.00	61.00	65.00	62.00	64.17 ± 2.56	
	S_f (dimensionless)	0.1–2	0.60	0.50	0.50	0.40	0.60	0.50	0.52 ± 0.08	
	w (m)	110–180	155.31	149.57	150.46	156.57	148.91	152.32	152.19 ± 3.15	
Second body (anomaly)	A_c (mV)	100–1500	581.30	576.40	580.70	578.10	582.50	572.80	578.63 ± 3.62	
	h (m)	0.5–80	3.20	3.40	3.60	2.90	3.80	3.50	3.40 ± 0.32	
	α ($^\circ$)	15–180	95.24	96.51	92.71	98.12	94.82	106.36	97.29 ± 4.79	
	S_f (dimensionless)	0.1–2	0.40	0.50	0.50	0.60	0.50	0.50	0.50 ± 0.06	
	w (m)	135–215	173.54	175.82	179.41	171.93	174.32	177.65	175.45 ± 2.76	
Third body (anomaly)	A_c (mV m)	100–4000	2335.60	2315.70	2289.30	2342.80	2297.10	2307.60	2314.68 ± 21.13	
	h (m)	0.5–40	7.40	7.80	8.40	7.60	7.90	7.70	7.80 ± 0.34	
	α ($^\circ$)	0–180	149.17	141.73	143.25	137.41	147.80	151.30	145.11 ± 5.22	
	S_f (dimensionless)	0.1–2	0.70	0.90	0.80	1.00	1.00	1.10	0.92 ± 0.15	
	w (m)	210–265	245.21	247.37	243.81	248.54	241.21	246.19	245.39 ± 2.63	

Table 7. Comparison of results obtained from different methods for the self-potential anomaly of sulfide deposit, Senneterre, Quebec, Canada

Model	Methods				
	Parameters	Santos (2010) and Gktrkler and Balkaya (2012) PSO method	Mehanee (2014) method	Biswas (2017) method	Present method
First body (anomaly)	A_c (mV)	454.94	219 to 224	189.5 ± 0.9	202.32 ± 5.78
	h (m)	5.6	9.7 to 10.2	7.6 ± 0.1	7.97 ± 0.38
	α ($^\circ$)	78.32	– 114 to – 117	61.0 ± 0.2	64.17 ± 2.56
	S_f (dimensionless)	0.48	0.5	0.50	0.52 ± 0.08
	w (m)	167.53	–	–	145.5 ± 0.1
Second body (anomaly)	A_c (mV)	2378.74	556	586.6 ± 1.8	578.63 ± 3.62
	h (m)	8.21	4	2.9 ± 0.0	3.40 ± 0.32
	α ($^\circ$)	150.51	– 83	93.8 ± 0.1	97.29 ± 4.79
	S_f (dimensionless)	1.1	0.5	0.50	0.50 ± 0.06
	w (m)	248.67	–	–	170.5 ± 0.0
Third body (anomaly)	A_c (mV m)	–	–	2574.8 ± 10.2	2314.68 ± 21.13
	h (m)	–	–	8.75 ± 0.0	7.80 ± 0.34
	α ($^\circ$)	–	–	146.9 ± 0.3	145.11 ± 5.22
	S_f (dimensionless)	–	–	1.0	0.92 ± 0.15
	w (m)	–	–	–	241.6 ± 0.1

The first horizontal gradient was then applied to the self-potential composite anomaly profile using different s values (window lengths) ($s = 2, 3, 4, 5, 6,$ and 7 m) (Fig. 5b); then, the global PSO technique was applied to these gradient anomalies to estimate the sheet model parameters using different ranges per parameter (Table 4). Table 4 shows the estimated parameters ($A_c, h, \beta, d,$ and w), where the errors of $A_c, h, \beta, d,$ and w were 0% and the RMS error was 0 mV. Table 4 shows that the proposed technique gives the best results of the model parameters, even if the model was contaminated with regional background.

To apply the proposed method to noisy data, 15% random noise was added to the previous synthetic model (Fig. 5c). The first horizontal gradient anomalies were calculated using the same previous window lengths ($s = 2, 3, 4, 5, 6,$ and 7 m) (Fig. 5d); then, by applying the PSO method to the gradient anomalies, the different parameters were estimated (Table 4). Table 4 shows the estimated parameters ($A_c = 202.11 \pm 15.61$ mV, $h = 12.03 \pm 0.14$ m, $\beta = 49.31 \pm 1.70^\circ$, $d = 6.03 \pm 0.55$ m, and $w = 9.90 \pm 0.41$ m), where the errors of $A_c, h, \beta, d,$ and w were 1.06%, 0.25%, 1.38%, 0.5% and 1%, respectively, and

the RMS error was 6.13 mV. Figure 5c compares the noisy and calculated anomalies.

Multi-model

The applicability and the efficiency of the used technique in estimating the multiple model parameters were tested. To do so, the method was applied to a composite anomaly composed of a sphere model with the following parameters: $S_f = 1.5$, $A_c = 4500$ mV m², $h = 3$ m, $\alpha = 60^\circ$, and $w = 0$ m—and a horizontal cylinder model with the following parameters: $S_f = 1$, $A_c = 3000$ mV m, $h = 9$ m, $\alpha = 30^\circ$, and $w = 30$ m (Fig. 6a). The profile length was 120 m, and the composite anomaly was obtained as:

$$V_{\text{comp}}(x_i, h, \alpha) = 4500 \frac{x_i \cos 60^\circ - 3 \sin 60^\circ}{(x_i^2 + 9)^{1.5}} + 3000 \frac{(x_i - 30) \cos 30^\circ - 9 \sin 30^\circ}{((x_i - 30)^2 + 81)}, i = 0, 1, 2, 3, \dots, M \quad (10)$$

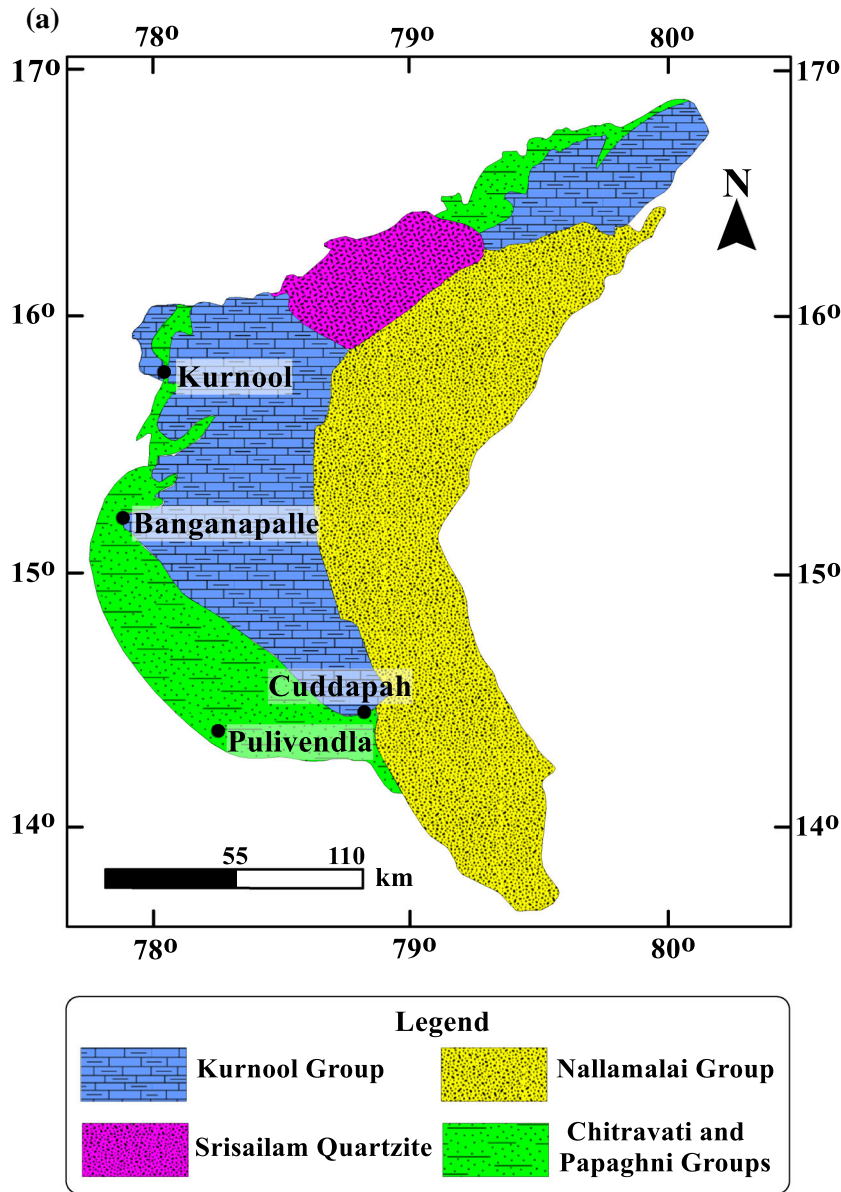


Fig. 8. Cuddapah basin, India: **a** Geological map (modified after Plumb 1981; Saha and Tripathy 2012). **b** Observed and estimated self-potential anomaly profile for the Kalava fault. **c** First horizontal gradient anomalies of the observed self-potential anomaly in **b**.

The first horizontal gradient was then applied to the composite anomaly profile using different s values ($s = 2, 3, 4, 5, 6,$ and 7 m) (Fig. 6b); then, the global PSO technique was applied to these gradient anomalies to estimate the multiple model parameters using different ranges for each parameter (Table 5). Table 5 shows the estimated parameters: ($A_c = 4523.2 \pm 31.65$ mV m², $h = 3.02 \pm 0.08$ m, $\alpha =$

$59.37 \pm 0.60^\circ$, $S_f = 1.53 \pm 0.05$, and $w = 0.013 \pm 0.02$ m) for the sphere model and $A_c = 3012.73 \pm 24.69$ mV m, $h = 9.08 \pm 0.13$ m, $\alpha = 30.19 \pm 0.40^\circ$, $S_f = 1.02 \pm 0.04$, and $w = 30.02 \pm 0.03$ m for the horizontal cylinder model. The errors of A_c , h , α , and S_f were 0.52%, 0.67%, 1.05%, and 2%, respectively, for the sphere model, whereas for the horizontal cylinder model, the errors of

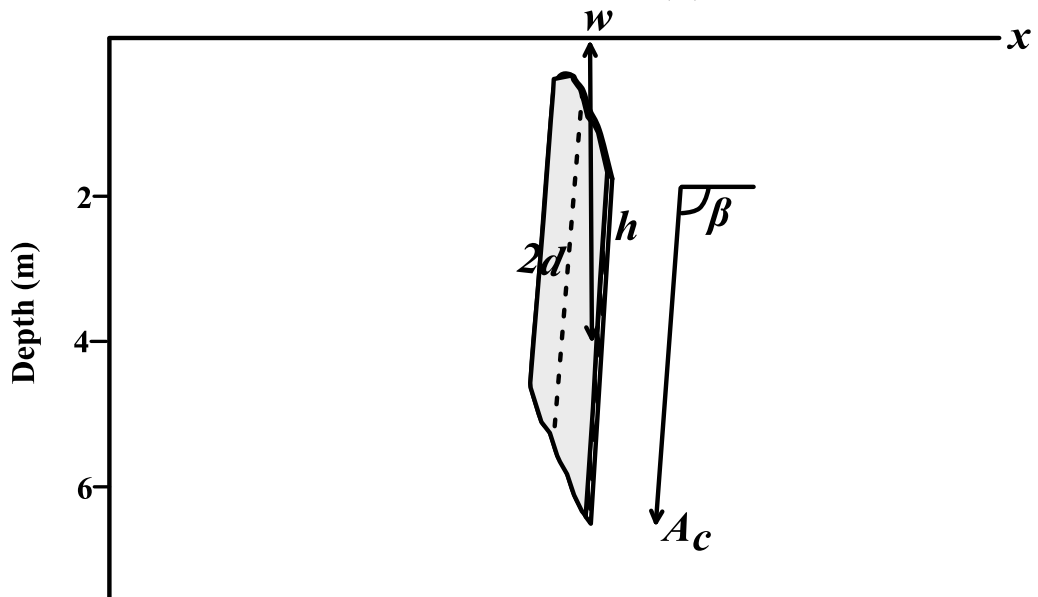
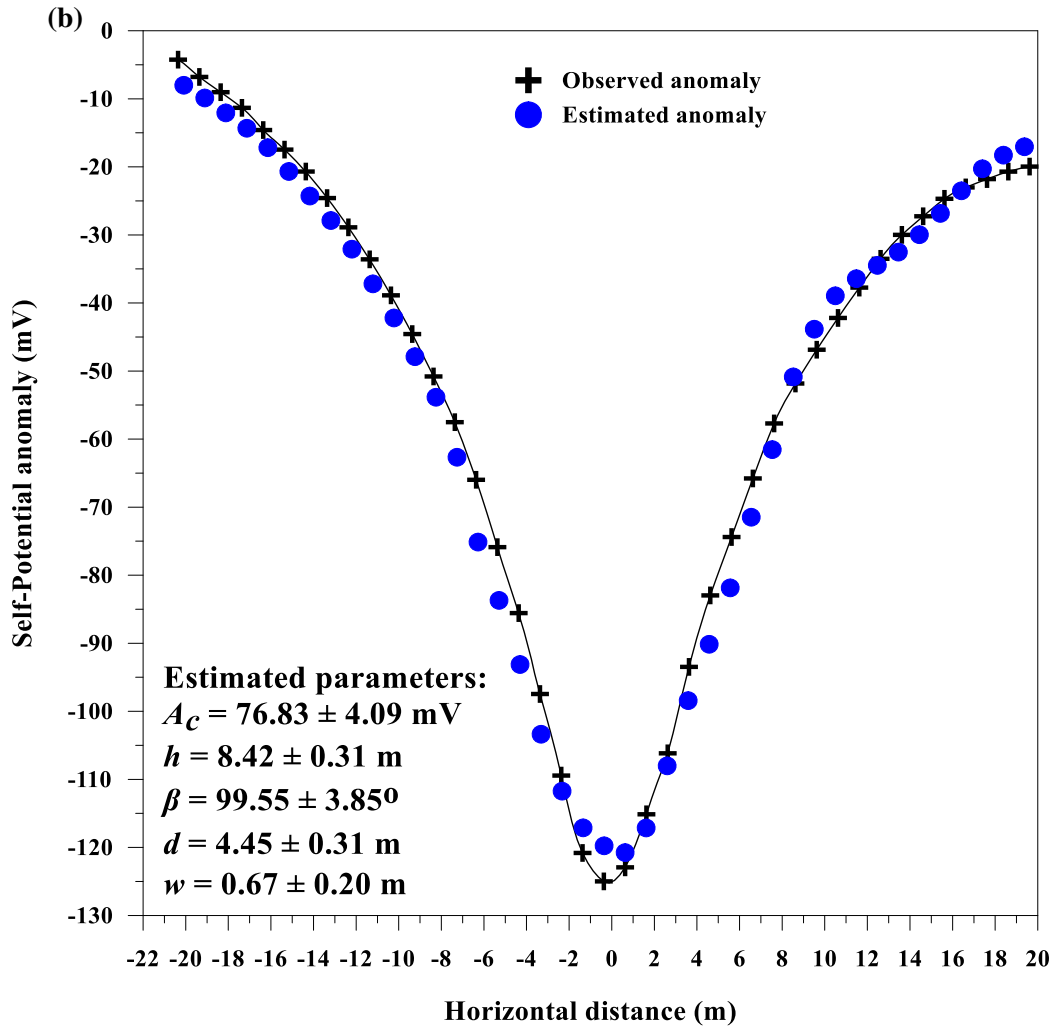


Fig. 8. continued.

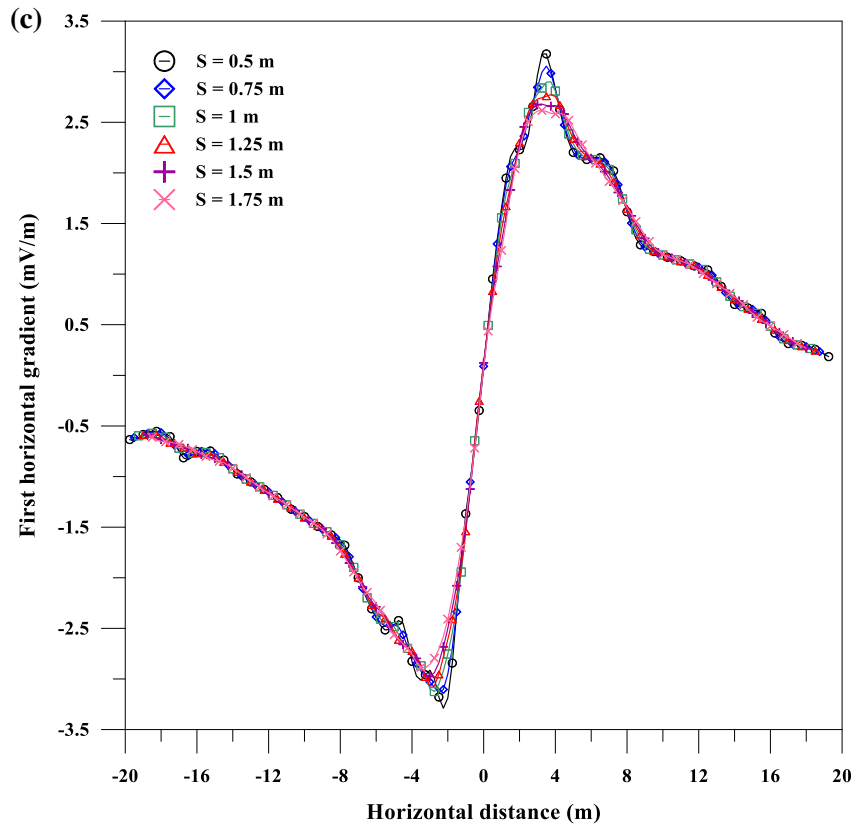


Fig. 8. continued.

Table 8. Results of the global PSO inversion algorithm applied to first horizontal gradient anomalies for the self-potential anomaly of Kalava fault, Cuddapah zone, India

Parameters	Used ranges	$s = 0.5$ m	$s = 0.75$ m	$s = 1$ m	$s = 1.25$ m	$s = 1.5$ m	$s = 1.75$ m	ϵ	RMS error (mV)
A_c (mV)	10–500	78.20	82.30	72.51	74.32	80.49	73.15	76.83 ± 4.09	4.14
h (m)	0.5–80	8.70	8.20	8.00	8.50	8.30	8.80	8.42 ± 0.31	
β ($^\circ$)	15–180	96.79	94.36	99.84	102.24	98.87	105.17	99.55 ± 3.85	
d (m)	0.5–35	4.70	4.20	4.90	4.50	4.10	4.30	4.45 ± 0.31	
w (m)	– 10–10	0.50	0.70	0.40	0.67	0.92	0.84	0.67 ± 0.20	

Table 9. Comparison of results obtained from different methods for the self-potential anomaly of Kalava fault, Cuddapah zone, India

Parameters	Methods						
	Murthy et al. (2005) method	Mehanee et al. (2011)	El-Kaliouby and Al-Garani (2009) method	Using Santos (2010) and Göktürkler and Balkaya (2012) PSO method	Mehanee (2014) method	Using Biswas and Sharma (2014a) method	Present method
A_c (mV)	–	–	68.29	67	617	65.84	76.83 ± 4.09
h (m)	9.38	3.65	7.2	7.9	5	7.14	8.42 ± 0.31
β ($^\circ$)	80.76	–	78.72	83.02	– 98	86.21	99.55 ± 3.85
d (m)	3.96	2.13	3.15	4.1	–	4.18	4.45 ± 0.31
w (m)	– 0.4	–	– 0.9	– 0.81	–	– 0.76	0.67 ± 0.20

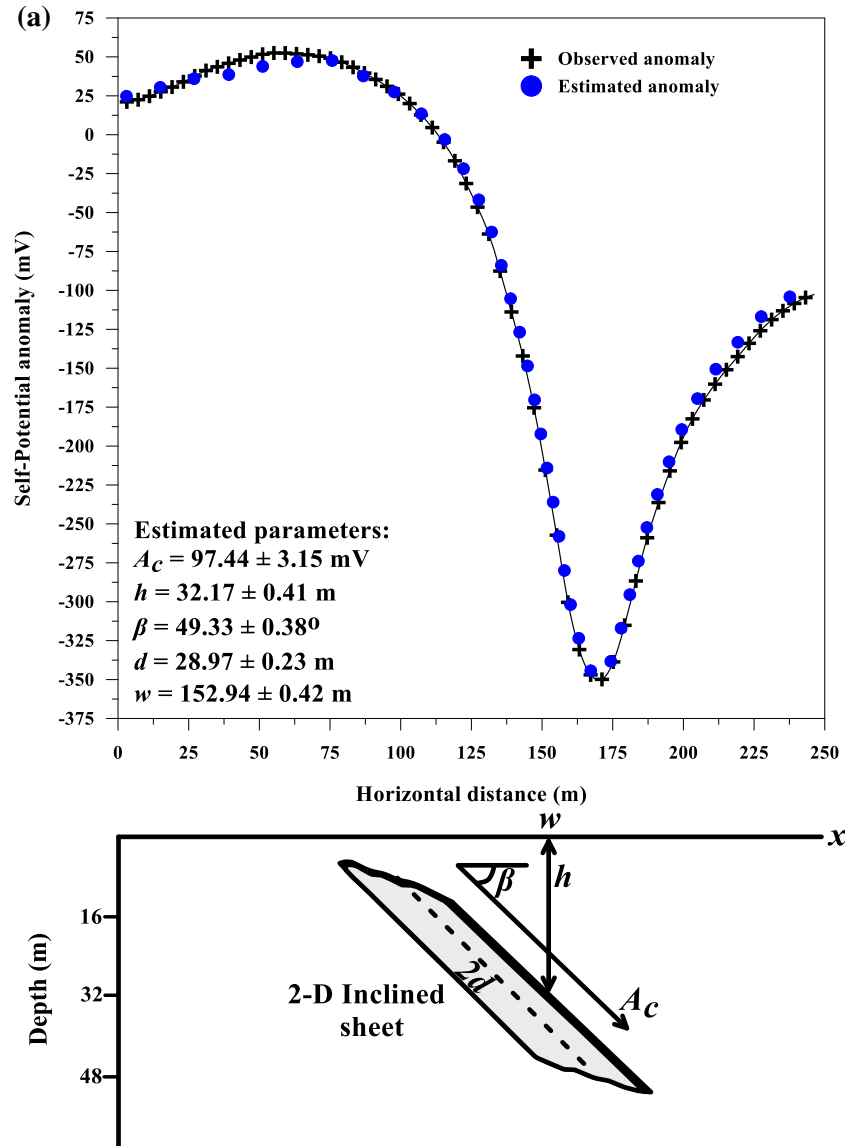


Fig. 9. Surda zone, India: **a** Observed and estimated self-potential anomaly profile for the copper sulfide deposit. **b** First horizontal gradient anomalies of the observed self-potential anomaly in **a**.

A_c , h , α , S_f , and w were 0.42%, 0.8%, 0.63%, 2%, and 0.07%, respectively, and the RMS error of the multiple model anomaly was 14.43 mV. Figure 6a shows the correlation between the multiple model anomaly and the estimated anomaly.

To apply the proposed method to noisy data, 15% random noise was added to the previous composite model (Fig. 6c). The first horizontal gradient anomalies were calculated using the same previous window lengths ($s = 2, 3, 4, 5, 6$, and 7 m) (Fig. 6d);

then, by applying the PSO method to the gradient anomalies, the different parameters were estimated (Table 5). Table 5 shows the estimated parameters: ($A_c = 4533.73 \pm 48.39 \text{ mV m}^2$, $h = 3.02 \pm 0.17 \text{ m}$, $\alpha = 60.73 \pm 2.38^\circ$, $S_f = 1.52 \pm 0.08$, and $w = -0.04 \pm 0.21 \text{ m}$) for the sphere model and ($A_c = 3030.95 \pm 47.09 \text{ mV m}$, $h = 8.95 \pm 0.26 \text{ m}$, $\alpha = 29.72 \pm 1.61^\circ$, $S_f = 1.03 \pm 0.08$, and $w = 30.14 \pm 0.28 \text{ m}$) for the horizontal cylinder model. The errors of A_c , h , α , and S_f were 0.75%, 0.67%, 1.22%, and

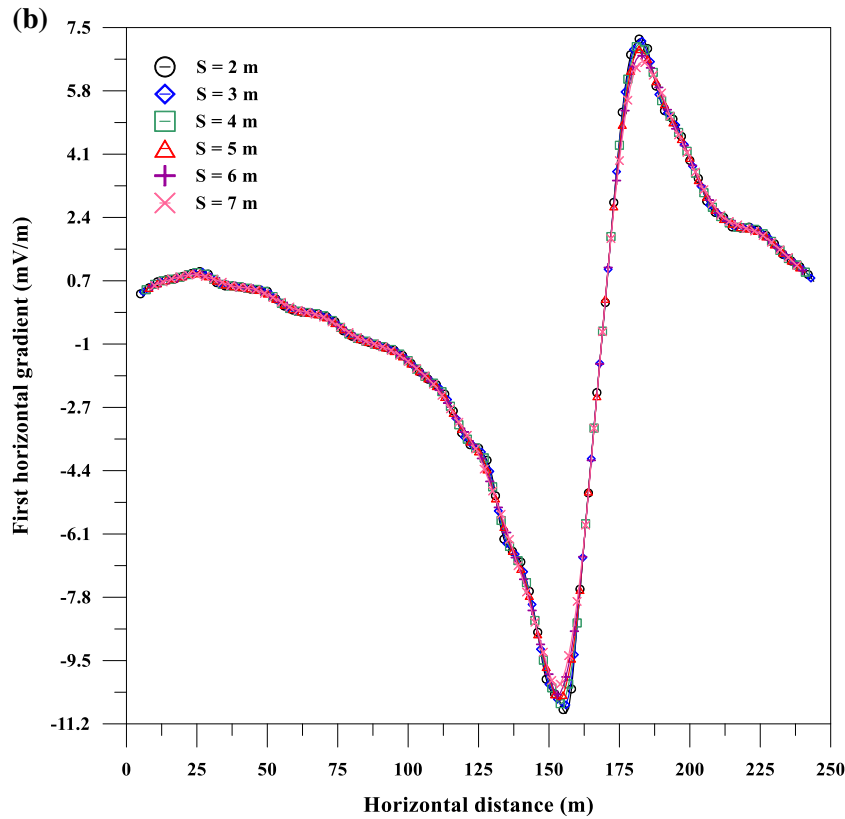


Fig. 9. continued.

Table 10. Results of the global PSO inversion algorithm applied to first horizontal gradient anomalies for the self-potential anomaly of copper sulfide deposit, Surda zone, India

Parameters	Used ranges	$s = 2$ m	$s = 3$ m	$s = 4$ m	$s = 5$ m	$s = 6$ m	$s = 7$ m	\mathcal{E}	RMS error (mV)
A_c (mV)	10–600	94.38	98.14	103.25	96.51	97.20	95.18	97.44 ± 3.15	5.86
h (m)	2–80	31.84	32.02	31.67	32.21	32.74	32.56	32.17 ± 0.41	
β ($^\circ$)	10–180	48.97	48.84	49.24	49.45	49.68	49.79	49.33 ± 0.38	
d (m)	5–45	29.12	28.94	28.87	28.73	28.82	29.35	28.97 ± 0.23	
w (m)	150–185	152.32	152.56	153.01	153.10	153.18	153.45	152.94 ± 0.42	

Table 11. Comparison of results obtained from different methods for the self-potential anomaly of copper sulfide Deposit, Surda Zone, India

Parameters	Methods				
	Murthy et al. (2005) method	El-Kaliouby and Al-Garani (2009) method	Santos (2010) method	Biswas and Sharma (2014a) method	Present method
A_c (mV)	–	130.86	98.38	107.8 ± 3.3	97.44 ± 3.15
h (m)	26.52	27.78	31.40	31.1 ± 0.2	32.17 ± 0.41
β ($^\circ$)	57.63	50.96	45.98	47.5 ± 0.4	49.33 ± 0.38
d (m)	19.81	19.51	28.8	26.1 ± 0.8	28.97 ± 0.23
w (m)	165.84	5.86	– 3.87	$- 1.2 \pm 0.5$	152.94 ± 0.42

1.33%, respectively, for the sphere model, whereas for the horizontal cylinder model, the errors of A_c , h , α , S_f , and w were 1.03%, 0.56%, 0.93%, 3%, and 0.47%, respectively, and the RMS error of the multiple model anomaly was 17.85 mV. Figure 6c compares the multiple model noisy anomaly and the estimated anomaly.

From the results shown above, the proposed method can be used to determine the multi-source parameters efficiently and accurately.

FIELD EXAMPLES

To examine the applicability and accuracy of the proposed algorithm in mining, the proposed technique was applied to three real field examples: one from Canada, which is the multi-source example, and two examples from India.

Self-potential Anomaly of Sulfide Deposit, Senneterre, Quebec, Canada (Multi-source)

Senneterre in Quebec is rich in minerals, in which pyrite and pyrrhotite account for approximately 30% of the entire zone, and the mineralized rocks that host pyrite and pyrrhotite are meta-sedimentary breccias and tuffs that are interbedded with lava flows (Telford et al. 1990; Biswas 2017). A self-potential anomaly profile was taken above the massive sulfide deposits (Telford et al. 1990; Biswas 2017). The profile length was 209 m, sampled at 1 m intervals (Fig. 7a). Figure 7a reveals that there were three anomalies. The self-potential profile was then filtered by the first horizontal gradient using different s values ($s = 2, 3, 4, 5, 6,$ and 7 m) (Fig. 7b). Then, the global PSO technique was applied to the first horizontal gradient anomalies to estimate the different parameters (A_c , h , α , S_f , and w) of the three anomalies using different ranges (Table 6); the calculated parameters were: $A_c = 202.32 \pm 5.78$ mV, $h = 7.97 \pm 0.38$ m, $\alpha = 64.17 \pm 2.56^\circ$, $S_f = 0.52 \pm 0.08$, and $w = 152.19 \pm 3.15$ m for the first anomaly; $A_c = 578.63 \pm 3.62$ mV, $h = 3.4 \pm 0.32$ m, $\alpha = 97.29 \pm 4.79^\circ$, $S_f = 0.5 \pm 0.06$, and $w = 175.45 \pm 2.76$ m for the second anomaly; and $A_c = 2314.68 \pm 21.13$ mV, $h = 7.8 \pm 0.34$ m, $\alpha = 145.11 \pm 5.22^\circ$, $S_f = 0.92 \pm 0.15$, and $w = 245.39 \pm 2.63$ m, for the third anomaly. The RMS error for the calculated self-potential field was 24.01 mV.

From the results shown in Table 6, we can conclude that the first and second bodies were vertical cylinders, whereas the third body was a horizontal cylinder. The correlation between the observed and calculated anomalies is shown in Fig. 7a. Table 7 compares the estimated parameters of the present method and those from other methods in the literature.

Kalava Fault, Cuddapah Zone, India

Cuddapah basin covers an area of approximately 35,000 km², with a maximum basin thickness at any point of approximately 6 km. It overlies the Archean basement (Plumb 1981). The Cuddapah basin comprises the following units (Plumb 1981; Saha and Tripathy 2012) (Fig. 8a). The Cuddapah Supergroup consists of the Papaghni, Chitravati, and Nallamalai Groups. The Papaghni Group is composed of fluvatile sandstone, conglomerate, flaggy buff dolomite, red to brown sandstone, and red siltstone. The Chitravati Group, which overlies disconformably the Papaghni Group, comprises Pulivendla quartzite, gray to green shale, flaggy sandstone, stromatolitic limestone (including thick dolerite sills), and Gandikota quartzite. The Nallamalai Group, which overlies unconformably the Chitravati Group, is composed of Bairenkonda quartzite, shale, phyllite, dolomite, and quartzite. The Cuddapah Supergroup is overlain unconformably by the Kurnool Group. The latter is composed of Banganapalle quartzite, Narji limestone, Auk shale, Paniam quartzite, Koilkuntla limestone, and Nandyal shale.

A self-potential anomaly profile was taken across the Kalava fault area, Cuddapah basin, India (Rao et al. 1982; Tlas and Asfahani 2008; El-Kaliouby and Al-Garani 2009) (Fig. 8b). The profile length was 40 m, which was sampled at 0.25 m. The self-potential profile was then filtered by the first horizontal gradient using different s values ($s = 0.5, 0.75, 1, 1.25, 1.5,$ and 1.75 m) (Fig. 8c). Then, the global PSO technique was applied to the horizontal gradient anomalies to estimate the different parameters (A_c , h , β , d , and w) using different ranges (Table 8), with the calculated parameters as follows: $A_c = 76.83 \pm 4.09$ mV, $h = 8.42 \pm 0.31$ m, $\beta = 99.55 \pm 3.85^\circ$, $d = 4.45 \pm 0.31$ m, and $w = 0.67 \pm 0.20$ m, and the RMS error was 4.14 mV. The correlation between the observed and calculated

anomalies is shown in Fig. 8b. Table 9 compares the estimated parameters of the present method and those from other methods in the literature.

Self-potential Anomaly of the Copper Sulfide Deposit, Surda Zone, India

The Surda area of the Rakha mines is endowed with copper sulfide deposits. These are located within the Singhbhum shear zone (Singhbhum copper belt), which extends to approximately 200 km from Duarparam in the western part to Baharagora in the southeastern part (Mishra et al. 2003).

A self-potential anomaly profile was taken above the copper sulfide deposits in Surda area, India (Murthy et al. 2005; Santos 2010; Biswas and Sharma 2014a) (Fig. 9a). The profile length was 243 m, and it was digitized at 1 m intervals. The first horizontal gradient filter was then applied to the self-potential anomaly profile using different s values ($s = 2, 3, 4, 5, 6,$ and 7 m) (Fig. 9b). Then, the global PSO technique was applied to the first horizontal gradient anomalies to estimate the different parameters ($A_c, h, \beta, d,$ and w) of the sheet using different ranges (Table 10). The calculated parameters were as follows: $A_c = 97.44 \pm 3.15$ mV, $h = 32.17 \pm 0.41$ m, $\beta = 49.33 \pm 0.38^\circ$, $d = 28.97 \pm 0.23$ m, and $w = 152.94 \pm 0.42$ m; and the RMS error was 5.86 mV. The correlation between the observed and calculated anomalies is shown in Fig. 9a. Table 11 compares the estimated parameters of the present method and those from other methods in the literature.

CONCLUSIONS

The applicability and the efficiency of the proposed technique (global PSO method applied to the first horizontal gradient) was explained and demonstrated for synthetic datasets and for real self-potential datasets from Canada and India. The method proposed here can be applied in mineral resource development, as it can be utilized to determine the different parameters (amplitude coefficient (A_c), depth (h), polarization angle (α), inclination angle (β), half-width (d), shape factor (S_f), and source origin (w)) of mineralized sources with different shapes (horizontal cylinder, vertical cylinder, sphere, and 2-D inclined sheet). A major

advantage of this method is that it removes regional background from the observed data such that the residual anomaly parameters are determined effectively. The global PSO provides fast convergence and does not require information regarding the source shape. However, the time needed to reach the global best solution increases when the number of models used in inversion increases, which can be considered a minor disadvantage of the method. The results obtained from the synthetic and real datasets show that the method is effective in interpreting self-potential data, even if there are multiple sources, and it can determine the parameters of the multiple sources. Finally, the results of the real field data are strongly comparable with those from other methods in the literature.

ACKNOWLEDGEMENTS

The author would like to thank Prof. Dr. John Carranza the Editor-in-Chief, and the reviewers of Natural Resources Research for their keen interest, valuable comments on the manuscript, and suggestions for improvements to this work.

REFERENCES

- Abdelrahman, E. M., El-Araby, T. M., & Essa, K. S. (2009a). Shape and depth determination from second moving average residual self-potential anomalies. *Journal of Geophysics and Engineering*, 6, 43–52.
- Abdelrahman, E. M., Essa, K. S., Abo-Ezz, E. R., & Soliman, K. S. (2006a). Self-potential data interpretation using standard deviations of depths computed from moving-average residual anomalies. *Geophysical Prospecting*, 54, 409–423.
- Abdelrahman, E. M., Essa, K. S., Abo-Ezz, E. R., Soliman, K. S., & El-Araby, T. M. (2006b). A least-squares depth-horizontal position curves method to interpret residual SP anomaly profiles. *Journal of Geophysics and Engineering*, 3, 252–259.
- Abdelrahman, E. M., Soliman, K. S., Essa, K. S., Abo-Ezz, E. R., & El-Araby, T. M. (2009b). A least-squares minimisation approach to depth determination from numerical second horizontal self-potential anomalies. *Exploration Geophysics*, 40, 214–221.
- Asfahani, J., & Tlas, M. (2005). A constrained nonlinear inversion approach to quantitative interpretation of self-potential anomalies caused by cylinders, spheres and sheet-like structures. *Pure and Applied Geophysics*, 162, 609–624.
- Asfahani, J., & Tlas, M. (2016). Interpretation of self-potential anomalies by developing an approach based on linear optimization. *Geosciences and Engineering*, 5, 7–21.
- Bhattacharya, B. B., & Roy, N. (1981). A note on the use of nomograms for self-potential anomalies. *Geophysical Prospecting*, 29, 102–107.

- Biswas, A. (2013). Identification and Resolution of Ambiguities in Interpretation of Self-Potential Data: Analysis and Integrated Study around South Purulia Shear Zone. India (Ph.D Thesis), Department of Geology and Geophysics, Indian Institute of Technology Kharagpur (p. 199). <https://www.idr.iitkgp.ac.in/xmlui/handle/123456789/3247>.
- Biswas, A. (2016). A comparative performance of least square method and very fast simulated annealing global optimization method for interpretation of self-potential anomaly over 2-D inclined sheet type structure. *Journal Geological Society of India*, 88, 493–502.
- Biswas, A. (2017). A review on modeling, inversion and interpretation of self-potential in mineral exploration and tracing paleo-shear zones. *Ore Geology Reviews*, 91, 21–56.
- Biswas, A., & Sharma, S. P. (2014a). Optimization of self-potential interpretation of 2-D inclined sheet-type structures based on very fast simulated annealing and analysis of ambiguity. *Journal of Applied Geophysics*, 105, 235–247.
- Biswas, A., & Sharma, S. P. (2014b). Resolution of multiple sheet-type structures in self-potential measurement. *Journal of Earth System Science*, 123, 809–825.
- Biswas, A., & Sharma, S. P. (2015). Interpretation of self-potential anomaly over idealized body and analysis of ambiguity using very fast simulated annealing global optimization. *Near Surface Geophysics*, 13(2), 179–195.
- Corwin, R. F., & Hoover, D. B. (1979). The self-potential method in geothermal exploration. *Geophysics*, 44, 226–245.
- Dmitriev, A. N. (2012). Forward and inverse self-potential modeling: a new approach. *Russian Geology and Geophysics*, 53, 611–622.
- Drahor, M. G. (2004). Application of the self-potential method to archaeological prospection: Some case histories. *Archaeological Prospection*, 11, 77–105.
- Eberhart, R. C., & Kennedy, J. (1995). A new optimizer using particle swarm theory. In: *Proceedings of the IEEE. The sixth Symposium on Micro Machine and Human Centre, Nagoya, Japan*, pp. 39–43.
- El-Kaliouby, H., & Al-Garni, M. A. (2009). Inversion of self-potential anomalies caused by 2D inclined sheets using neural networks. *Journal of Geophysics and Engineering*, 6, 29–34.
- Essa, K. S. (2007). Gravity data interpretation using the s-curves method. *Journal of Geophysics and Engineering*, 4, 204–213.
- Essa, K. S. (2011). A new algorithm for gravity or self-potential data interpretation. *Journal of Geophysics and Engineering*, 8, 434–446.
- Essa, K. S. (2019). A particle swarm optimization method for interpreting self-potential anomalies. *Journal of Geophysics and Engineering*, 16, 463–477.
- Essa, K. S. (2020). Self-potential data interpretation utilizing the particle swarm method for the finite 2D inclined dike: Mineralized zones delineation. *Acta Geodaetica et Geophysica*. <https://doi.org/10.1007/s40328-020-00289-2>.
- Essa, K. S., & Elhussein, M. (2017). A new approach for the interpretation of self-potential data by 2-D inclined plate. *Journal of Applied Geophysics*, 136, 455–461.
- Essa, K. S., & Elhussein, M. (2018). PSO (particle swarm optimization). For interpretation of magnetic anomalies caused by simple geometrical structures. *Pure and Applied Geophysics*, 175, 3539–3553.
- Essa, K. S., & Elhussein, M. (2020). Interpretation of magnetic data through particle swarm optimization: Mineral exploration cases studies. *Natural Resources Research*, 29(1), 521–537.
- Essa, K. S., Mehane, S., & Smith, P. (2008). A new inversion algorithm for estimating the best fitting parameters of some geometrically simple body from measured self-potential anomalies. *Exploration Geophysics*, 39, 155–163.
- Fedi, M., & Abbas, M. A. (2013). A fast interpretation of self-potential data using the depth from extreme points method. *Geophysics*, 78, E107–116.
- Fernandez-Martinez, J., Garcia-Gonzalo, E., & Naudet, V. (2010). Particle swarm optimization applied to solving and appraising the streaming potential inverse problem. *Geophysics*, 75, WA3–WA15.
- Göktürkler, G., & Balkaya, Ç. (2012). Inversion of self-potential anomalies caused by simple-geometry bodies using global optimization algorithms. *Journal of Geophysics and Engineering*, 9, 498–507.
- Kawada, Y., & Kasaya, T. (2018). Self-potential mapping using an autonomous underwater vehicle for the Sunrise deposit, Izu-Ogasawara arc, southern Japan. *Earth, Planets and Space*, 70, 142.
- Mehane, S. (2014). An efficient regularized inversion approach for self-potential data interpretation of ore exploration using a mix of logarithmic and non-logarithmic model parameters. *Ore Geology Reviews*, 57, 87–115.
- Mehane, S. (2015). Tracing of paleo-shear zones by self-potential data inversion: case studies from the KTB, Rittsteig, and Grossensees graphite-bearing fault planes. *Earth, Planets and Space*, 67, 14–47.
- Mehane, S. A., & Essa, K. S. (2015). 2.5D regularized inversion for the interpretation of residual gravity data by a dipping thin sheet: Numerical examples and case studies with an insight on sensitivity and non-uniqueness. *Earth, Planets and Space*, 67, 130.
- Mehane, S., Essa, K. S., & Smith, P. D. (2011). A rapid technique for estimating the depth and width of a two-dimensional plate from self-potential data. *Journal of Geophysics and Engineering*, 8, 447–456.
- Minsley, B. J., Coles, D. A., Vichabian, Y., & Morgan, F. D. (2008). Minimization of self-potential survey mis-ties acquired with multiple reference locations. *Geophysics*, 73, F71–F81.
- Mishra, B., Pal, N., & Ghosh, S. (2003). Fluid evolution of the mosabani and rakha copper deposits, Singhbhum District, Jharkhand: Evidence from fluid inclusion study of mineralized quartz veins. *Journal Geological Society of India*, 61, 51–60.
- Murthy, B. V. S., & Haricharan, P. (1985). Nomograms for the complete interpretation of spontaneous potential profiles over sheet like and cylindrical 2D structures. *Geophysics*, 50, 1127–1135.
- Murthy, I. V. R., Sudhakar, K. S., & Rao, P. R. (2005). A new method of interpreting self-potential anomalies of two-dimensional inclined sheets. *Computers & Geosciences*, 31, 661–665.
- Parsopoulos, K. E., & Vrahatis, M. N. (2002). Recent approaches to global optimization problems through particle swarm optimization. *Natural Computing*, 1, 235–306.
- Paul, M. K. (1965). Direct interpretation of self-potential anomalies caused by inclined sheets of infinite extension. *Geophysics*, 30, 418–423.
- Plumb, K. A. (1981). Workshop: Comparison of the Cuddapah basin, India and the Adelaide Geosyncline, Australia, Report of overseas visit. In: *Bureau of mineral resources, geology and geophysics, Record*.
- Rao, A. D., Babu, H., & Sivakumar Sinha, G. D. (1982). A Fourier transform method for the interpretation of self-potential anomalies due to two-dimensional inclined sheet of finite depth extent. *Pure and Applied Geophysics*, 120, 365–374.
- Roudsari, M. S., & Beitollahi, A. (2013). Forward modelling and inversion of self-potential anomalies caused by 2D inclined sheets. *Exploration Geophysics*, 44, 176–184.
- Saha, D., & Tripathy, V. (2012). Palaeoproterozoic sedimentation in the Cuddapah Basin, South India and regional tectonics—a

- review. In R. Mazumder & D. Saha (Eds.), *Paleoproterozoic of India, Geological Society, London* (Vol. 365, pp. 159–182). London: Special Publication.
- Santos, F. A. (2010). Inversion of self-potential of idealized bodies' anomalies using particle swarm optimization. *Computers & Geosciences*, 36, 1185–1190.
- Sen, M. K., & Stoffa, P. L. (2013). *Global optimization methods in geophysical inversion*. Cambridge: Cambridge University Press.
- Sharma, S. P., & Biswas, A. (2013). Interpretation of self-potential anomaly over 2D inclined structure using very fast simulated annealing global optimization—An insight about ambiguity. *Geophysics*, 78, 3–15.
- Singh, A., & Biswas, A. (2016). Application of global particle swarm optimization for inversion of residual gravity anomalies over geological bodies with idealized geometries. *Natural Resources Research*, 25, 297–314.
- Stoll, J., Bigalke, J., & Grabner, E. W. (1995). Electrochemical modelling of self-potential anomalies. *Surveys in Geophysics*, 16, 107–120.
- Sundararajan, N., Arun Kumar, I., Mohan, N. L., & Seshagiri Rao, S. V. (1990). Use of Hilbert transform to interpret self-potential anomalies due to two-dimensional inclined sheets. *Pure and Applied Geophysics*, 133, 117–126.
- Sundararajan, N., SrinivasaRao, P., & Sunitha, V. (1998). An analytical method to interpret self-potential anomalies caused by 2D inclined sheets. *Geophysics*, 63, 1551–1555.
- Tarantola, A. (2005). *Inverse problem theory and methods for model parameter estimation*. Society for Industrial and Applied Mathematics (SIAM), Philadelphia.
- Telford, W. M., Geldart, L. P., & Sheriff, R. E. (1990). *Applied geophysics*. London: Cambridge University Press.
- Tlas, M., & Asfahani, J. (2008). Using of the adaptive simulated annealing (ASA) for quantitative interpretation of self-potential anomalies due to simple geometrical structures. *Journal of King Abdulaziz University Earth Sciences*, 19, 99–118.
- Venter, G., & Sobieski, J. (2002). Particle swarm optimization. In *AIAA 2002-1235, 43rd AIAA/ASME/ASCE/AHS/ASC structures, structural dynamics, and materials conference*, Denver, CO.
- Vichabian, Y., & Morgan, F. D. (2002). Self-potentials in cave detection. *The Leading Edge*, 21, 866–871.
- Wang, Y. (2016). *Seismic inversion: Theory and applications*. New York: Wiley-Blackwell.
- Wynn, J. C., & Sherwood, S. I. (1984). The self-potential (SP) method: An inexpensive reconnaissance archaeological mapping tool. *Journal of Field Archaeology*, 11(2), 195–204.
- Zhdanov, M. S. (2002). *Geophysical inversion theory and regularization problems*. Amsterdam: Elsevier.